Disponible en ligne sur www.sciencedirect.com
ScienceDirect
C. R. Chimie 13 (2010) 69–96
COMPTES RENDUS CHIMIE

Full paper/Mémoire

Full spectroscopic characterization of an hydrolytically stable and colored Ti(IV)-precursor in solution

Hamid Senouci [a], Bérénice Millet [a], Christophe Volkringer [b], Clarisse Huguenard [a], Francis Taulelle [b], Marc Henry [a,*]

[a] *Laboratoire de chimie moléculaire de l'état solide, UMR CNRS/UdS 7140, institut Le Bel, université de Strasbourg, 4, rue Blaise-Pascal, 67070 Strasbourg cedex, France*

[b] *Institut Lavoisier, UMR CNRS 8180, université de Versailles-Saint-Quentin-en-Yvelines, 45, avenue des États-Unis, 78035 Versailles, France*

Reçu le 28 mars 2009 ; accepté après révision le 4 novembre 2009

Abstract

The orange-colored and hydrolytically stable compound $\{[Ti_2O(bhmpc)(Hbhmpc)(H_2bhmpc)].C_4H_8O_2.HX\}_2$ (with H_3bhmpc = 2,6-bis(hydroxymethyl)-*p*-cresol and X = OEt or CCl_3) has been studied by a combination of single crystal X-ray diffraction data, U.V.-vis. spectroscopy, IR and Raman spectroscopies, ^1H, ^{13}C and ^{17}O solution NMR spectroscopies, electron density and statistical thermodynamics modeling. We observed that the molecular structure found in the solid state is conserved in solution. Based on X-ray diffraction data, we also propose a complete and non-ambiguous assignment for the fully resolved ^1H and ^{13}C solution NMR spectra through the use of 2D-techniques (COSY, ROESY, HSQC, HMBC) and ^1H relaxation time measurements. The ability of the partial charge model introduced more than 20 years ago by J. Livage's group to reproduce observed ^{13}C NMR chemical shifts in solution is demonstrated. Statistical thermodynamic modeling between $Ti(OR)_4$ (monomers, trimers or tetramers) has shown that complexation was in all cases under entropy control. Possible applications of this soluble and stable precursor to the sol–gel processing of hybrid organic–inorganic are addressed. ***To cite this article: H. Senouci et al., C. R. Chimie 13 (2010).***

Keywords: U.V.-Vis. spectroscopy; IR and Raman spectroscopy; NMR; ^1H; ^{13}C; ^{17}O; COSY; ROESY; HSQC; HMBC; PACHA; Ti(IV) aryloxides; 2,6-bis(hydroxymethyl)-*p*-cresol; Hybrid organic-inorganic materials; PACHA modeling; Statistical thermodynamics

1. Introduction

Titanium dioxide TiO_2 is a strategic material in many fields of materials chemistry [1]. Owing to its large refractive index (n_D = 2.7 and 2.55 at 590 nm for rutile and anatase polymorphs respectively), it is widely used for making white pigments [2] or high-refractive-index coatings on silica glasses [3]. With its well-sized band gap (E_g = 3.1–3.2 eV) [4], it may be used in the photoelectrolysis of water [5] and leads to economically credible photocatalysts [6], gas sensors [7] or photovoltaic devices [8]. Moreover, upon UV irradiation TiO_2-containing materials may become superhydrophilic leading to self-cleaning materials

* Corresponding author.
Adresses e-mail: volkringer@chimie.uvsq.fr (C. Volkringer), huguenar@chimie.u-strasbg.fr (C. Huguenard), taulelle@chimie.uvsq.fr (F. Taulelle), henry@chimie.u-strasbg.fr (M. Henry).

1631-0748/$ – see front matter
doi:10.1016/j.crci.2009.11.008

[9]. When mixed with an alkaline earth oxide (MgO, CaO, SrO, BaO), TiO_2 leads to a wide array of ferroelectric [10], piezoelectric [11] and pyroelectric [12] high-tech ceramics for electronic applications. Finally, if mixed with polymers, original organic–inorganic hybrid materials may be readily obtained, combining in a single phase important properties such as high transparency (glasslike), low temperature processing (polymer-like) and sufficient thermal stability (ceramic-like) [13]. In all the above applications, the starting molecular precursors of titanium oxide are usually titanium tetra-alkoxides mixed with various chemical additives in order to finely tune the hydrolytic behavior of these highly reactive species and the final processing of the resulting sol or gel phase [1]. The pioneer work of J. Livage's group in this domain is worth noticing and was initiated by suggestion from André Vioux about the use of acetic acid in order to monitor and control the hydrolysis and condensation of titanium(IV) alkoxides in order to obtain monolithic TiO_2 gels under reproducible conditions [14]. Thanks to the top-level expertise of J. Livage's group in spectroscopy, it was then quickly demonstrated through the use of ESR [15], IR [16], XANES/EXAFS [17] and ^{13}C CPMAS NMR [18] that a change of coordination number from 4 or 5 in $Ti(OR)_4$ up to 6 in $TiO_x(OR)_y(OAc)_z$ derivatives was the key point allowing orientation of the polycondensation process leading to Ti—O—Ti bonds towards a gel instead of a precipitate. With the use of acetic acid as a gelling agent, it was thus possible to synthesize not only homogenously Cr^{3+} and Al^{3+}-doped TiO_2 photoanodes for the photoelectrolysis of water [19] but also to initiate a very fundamental research through the establishment of a Partial Charge Model (PCM) putting onto a quantitative basis some crucial ideas concerning the nature of the chemical bond along the lines suggested by L. Pauling or R.T. Sanderson [20–23]. It is worth noting that this PCM approach of chemical reactivity has been validated by other groups in the case of antimonates, phosphates, molybdates, ferrates or stannates [24], silicates [25], aluminates [26] but seems to fail in the case of alkoxides bearing a lone pair such as tellurium alkoxides $Te(OR)_4$ [27]. With the help of this PCM, it was thus possible to rationalize the solution and sol–gel chemistry of most metallic species in both aqueous and non-aqueous solvents based on the sole knowledge of stoichiometric coefficients. On one hand, this was a great advantage, as in most cases, the detailed molecular structure in solution or the gel state remains unknown. On the other hand, it was soon realized by working at low hydrolysis ratios ($h = H_2O/Ti < 1$) that single-crystals could be easily grown from solutions allowing a much better understanding of the structural chemistry involved during the very first steps of a titania-based sol–gel process. The original PCM approach, unable to take into account the detailed molecular structure was thus regarded with more and more scepticism, more particularly by people deeply involved in NMR spectroscopy or in *ab initio* calculations. A survey of the literature devoted to NMR studies of crystalline titanium(IV) oxo-alkoxides show that four types of nuclei have been studied: ^{1}H, ^{13}C, ^{17}O and $^{47,49}Ti$. Very few results have been reported concerning ^{47}Ti and ^{49}Ti NMR owing to the rather large quadrupolar moment of these two nuclei. This comes from the fact that TiO_6 or TiO_5 polyhedra are usually strongly distorted relative to their corresponding ideal regular geometry leading to large electrical field gradients at the titanium center and thus to very broad signals. Consequently, titanium NMR is limited to symmetric tetrahedral species, such as $TiCl_4$ (NMR reference) or $Ti(O^iC_3H_7)_4$ and $Ti(OCH_2{}^tC_4H_9)_4$, characterized by $\delta(^{49}Ti) = -854$ ppm and $\delta(^{47}Ti) = -1120$ ppm [28]. Owing to the fast exchange between terminal and bridging positions, ^{17}O NMR is not very informative for non-hydrolyzed titanium alkoxides that are just characterized by a deshielding of about 250 ppm from the parent alcohol [29–30]. This is no more true for titanium oxo-alkoxides where a very clear differentiation between oxo groups is usually observed: $\delta(OTi_2) = 650–850$ ppm, $\delta(OTi_3) = 450–650$ ppm and $\delta(OTi_4,OTi_5) = 250–450$ ppm [31,32]. These characteristic signatures may thus be used to follow the start of these oxo cores during the design and synthesis of hybrid organic–inorganic materials [32]. However, a severe limitation of the technique comes from the fact that only a few signals are usually observed and that natural abundance ^{17}O NMR can be performed only on non-viscous solutions. For gels or xerogels where solid state NMR is required, isotope enrichment is mandatory, preventing tone performing routine analysis on these compounds. ^{1}H NMR techniques are also not very convenient owing to the very limited chemical shift range and to large dipolar couplings in the solid state. In solution one usually get either quite deceptive spectra in the fast exchange limit (0.5–0.7 ppm deshielding relative to the parent alcohol for Ti—O—CH_x protons) or very complex spectra in the slow exchange limit owing to the numerous scalar couplings. Consequently, with its one-half spin associated to a large chemical shift range and dilute

spin situation, the best nucleus remains ^{13}C owing to the easy routine access to high-resolution spectra both in solution and in the solid state. A survey of literature shows that if well resolved ^{13}C NMR spectra are very often reported for titanium oxo-alkoxides a complete attribution of the observed signals is rarely given. This comes from the fact that these polynuclear crystalline complexes are quite sensitive to moisture and usually obtained with very small yields, preventing one to perform detailed NMR studies. With this background in mind, the aims of this contribution written to celebrate the 70th anniversary of J. Livage are the following.

Perform a full spectroscopic study of a tetranuclear Ti(IV) complex absorbing in the visible part of the electromagnetic spectrum that may be routinely obtained with large yields and displaying very good hydrolytic stability [33]. One of the main application for such a molecular precursor would be to dispose of a stable $\{Ti_4O_{16}\}$ inorganic core that could be used (with or without further functionalization) in hybrid organic–inorganic devices relying of the well-known properties associated with the existence of Ti—O—Ti bonds. Accordingly, by shifting the edge of light absorption from the UV range towards the visible range, a considerable enhancement of the quantum yield for the conversion of light into electricity or of the photocatalytic properties may be anticipated. Moreover, being perfectly stable and inert towards moisture, this precursor could be used in any kind of sol–gel process in big contrast with more reactive and labile titanium(IV) (oxo)-alkoxides.

Another aim of this paper is to show that the PCM approach, 20 years after its first introduction in close collaboration with J. Livage, has been considerably improved to a level where prediction of ^{13}C NMR shifts directly from the knowledge of the molecular structure becomes possible. Accordingly, computation of ^{13}C NMR shifts is a considerable scientific challenge owing to the well-known extraordinary sensitivity of this nucleus to any change of the structure. The ability to reproduce experimental shifts is thus a very stringent test of the validity and quality of the partial charges distributions computed from an electronegativity equalization principle. In order to perform such a demonstration, we must dispose of a stable polynuclear Ti(IV) complex giving rise to a large number of ^{13}C NMR lines. The molecular structure of titanium(IV) alkoxides in solution is also a major concern in sol–gel chemistry and we will show how to handle this difficult problem with the PACHA approach using a rigorous statistical thermodynamic approach.

2. Materials and methods

2.1. Synthesis

In order to get reproducible NMR spectra, the synthesis of a previously reported [33] titanium(IV) oxo-aryloxide (**1**) has been optimized:

$$4Ti(OEt)_4 + 6H_3bhmpc + 2H_2O + 2\,C_4H_8O_2 \rightarrow 14EtOH + \{[Ti_2O(bhmpc)(Hbhmpc)(H_2bhmpc)].C_4H_8O_2.EtOH\}_2(\mathbf{1})$$

First, a solution made from 15 ml of 1,4-dioxane and 5 ml of ethanol and containing 0.8 g (4.76 mmol) of 2,6-bis(hydroxymethyl)-*p*-cresol (H_3bhmpc, 4.76 mmol) and 0.021 mL (1.20 mmol) of water was prepared. After complete dissolution of the ligand, 0.5 ml (2.38 mmol) of $Ti(OEt)_4$ were added under a nitrogen atmosphere in a plastic bag. The resulting orange solution was magnetically stirred for 10 minutes and then left overnight leading to an abundant precipitation of orange-colored rod-shaped crystals. Fig. 1 (top left) shows that (**1**) is a centro-symmetric molecule built from a planar $\{Ti_4(\mu_3\text{-}O)_2\}$assembly of four TiO_6 octahedra sharing edges and surrounded by three pairs of aromatic ligands. The overall shape of (**1**) may be described as a doubly fused calix[3]arene (Fig. 1, bottom left) where the organic joints have been replaced by Ti-atoms. Owing to the existence of these two divergent cavities and to the fact that aromatic ligands are found under three different protonation states (bhmpc, Hbhmpc and H_2bhmpc), solvent molecules (dioxane and ethanol) are found to be associated through hydrogen bonds to the complex (Fig. 1, right). The complete energetic characterization of both the intra- and intermolecular H-bonding scheme in this kind of complex has been studied elsewhere [1,33]. It is worth noticing that another structure may be obtained after recrystallization of **(1)** in $CHCl_3$, where $CHCl_3$ molecules are trapped instead of EtOH [33]. This structure exhibits two non-equivalent complexes per unit cell, differing essentially by their interactions with solvent molecules, but with the same molecular structure, identical to the molecular entity found in the as-synthesized compound. As explained above, the correlation between the electronic densities derived from the crystalline structure of **(1)** in the solid state and the NMR parameters measured when **(1)** in dissolved in $CDCl_3$ will also be studied. Thus, it was assumed that the presence of the interaction between the complex and EtOH (in the solid) or its absence (when the complex is surrounded by $CDCl_3$ molecules in solution) does not

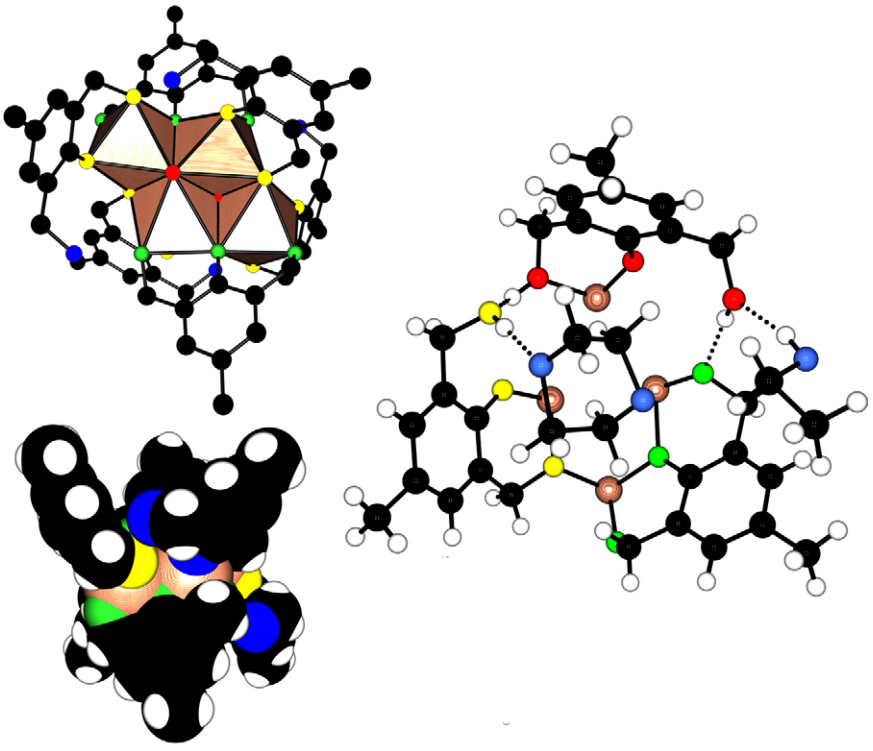

Fig. 1. Molecular structure of $\{[Ti_2O(bhmpc)(Hbhmpc)(H_2bhmpc)].C_4H_8O_2.EtOH\}_2$ (**1**) where H_3bhmpc would stand for 1,3-bis(hydroxymethyl)-p-cresol. Top: Association of four TiO_6 octahedral units and coordination of the ligands. Bottom: double calix shape of the complex. Middle: only one ligand of each type is represented to show hydrogen bonding between Hbhmpc (yellow) and dioxane and between H_2bhmpc (red) and ethanol. Oxygen atoms of solvents are blue colored. Also shown intramolecular hydrogen bonding between H_2bhmpc (red) and Hbhmpc (yellow), H_2bhmpc and bhmpc (green).

influence too much electronic densities at C-sites, so that calculations based on solid-state structures can be reasonably correlated to ^{13}C parameters of the complex in solution. As will be discussed below, this rough assumption appears to be valid for the majority of the complex C sites, as few of them are under strong influence of the solvent molecules in any case.

Orange-colored crystalline powders may also be obtained by adding to a solution of 6 mL of $Ti(OPr^i)_4$ in 5 mL of isopropanol, a solution of 0.67 g of H_3bhmpc dissolved in 15 mL of 1,4-dioxane and 3.17 μL of water. The same protocol using 6 g of $Ti(OBu^n)_4$ in 5 mL of butanol-1 and 0.59 g of H_3bhmpc has also led to orange-colored crystalline powders. In all cases, these crystals were found to be too small for performing a structure determination through single-crystal X-ray diffraction.

2.2. U.V.-Vis. spectroscopy

Spectra of the free ligand and of the complex after dissolution in $CHCl_3$ have been recorded on a Varian Multicell Block for Cary 1/3 spectrophotometer at a concentration of $7{\cdot}10^{-4}$ M.

2.3. IR and Raman spectroscopy

FT-IR spectra were recorded on KBr pellets between 400–4000 cm^{-1} on a Perkin-Elmer 1600 spectrometer. Micro-Raman measurements have been made on a Renishaw microscope, Ramascope model, equipped with 200 mW Ar^+ blue laser ($\lambda = 488$ nm). The best resolution (1 cm^{-1}) was obtained by recording four spectra (0–4000 cm^{-1}) using each time a 1000 cm^{-1} range. Signals below 200 cm^{-1} were filtered with the Rayleigh line and were not observed. Calibration of the microscope for the 0–1000 cm^{-1} range was made on a silicon wafer (520.1 cm^{-1} line). Microcrystalline powders were observed (×50 magnification) without any special preparation after deposition on a glass wafer. For each powder, acquisition of the spectra was made on at least four different crystallites with acquisition times within a 5–60 s range.

2.4. NMR

^{17}O NMR spectra were recorded on a Bruker spectrometer operating at 400 MHz for ^1H and

44.2 MHz for ^{17}O after dissolution of 26 mg of (**1**) in $CDCl_3$ (3.2 g). Owing to the low solubility of (**1**) in $CDCl_3$, the solution has been filtered before filling the 10 mm NMR tube preventing the computation of the real concentration. Acquisition time was 12 h for 221,694 scans using a 0.1 s repetition time.

^1H MAS and $^{13}C\{^1H\}$ CPMAS NMR measurements were performed using a Bruker Avance-300 spectrometer, operating at 300.33 MHz for ^1H and 75.52 MHz for ^{13}C (spectra 1 and 2 on Figs. 6 and 7), or a Bruker Avance-500 spectrometer, operating at 500.03 MHz for ^1H and 125.73 MHz for ^{13}C (spectra 3 to 5 on Figs. 6 and 7), both equipped with 4 mm H-X probes. The samples were rotated at, respectively, ν_R = 10 kHz with corresponding CPMAS magnetization transfer conditions $\nu_{RF}(^1H)$ = 32.5 kHz and $\nu_{RF}(^{13}C)$ = 42.5 kHz or rotated at 13 kHz with $\nu_{RF}(^1H)$ = 45.7 kHz and $\nu_{RF}(^{13}C)$ = 32.7 kHz, using a 2.5 ms contact time in both cases. ^1H decoupling composite pulse sequences used were spinal64 for measurements performed on Avance-300 and tppm180 on Avance-500 spectrometers. Other acquisition parameters were typically eight scans using a 10 s repetition time for ^1H MAS and for $^{13}C\{^1H\}$ CPMAS, 1024 to 2048 scans using a 5 s repetition time.

All ^1H and ^{13}C solution NMR measurements were performed at room temperature on a solution of (**1**) (5 mg) in $CDCl_3$ (0.6 mL) using a Bruker Avance-500 spectrometer, operating at 500.13 MHz for ^1H and 125.7 MHz for ^{13}C, equipped with a $^1H/^{13}C$ 5 mm gradient-probe. We used a gradient selected version (gs-) for each type of 1D and 2D pulse sequence except for ROESY. The solvent signal was taken as a secondary reference for ^1H and ^{13}C chemical shift (7.26 ppm for C^1HCl_3 residue and 77 ppm for $^{13}CDCl_3$, relative to TMS). In addition to classical 1D ^1H and ^{13}C $\{^1H\}$ spectra, four types of 2D spectra were collected: a ^1H—^1H scalar correlation spectrum, recorded using a gs-DQFCOSY pulse sequence, two scans, 2.5 s as repetition time, and 512 increments for indirect dimension; a ^1H—^1H dipolar correlation spectrum, recorded with a ROESY pulse sequence, 16 scans, 2.5 s as repetition time, 512 increments for indirect dimension and a total mixing spin-lock duration of 300 ms suitable for the correlation time one can expect, considering the size of the molecular entity under study; a ^1H—^{13}C via $^1J_{C—H}$ scalar correlation spectrum, acquired with a gs-HSQC pulse sequence, eight scans, 2 s as repetition time, 1024 increments in ^{13}C dimension and a delay 1/4J = 1.56 ms corresponding to mean $^1J_{C—H}$ = 160 Hz; a ^1H—^{13}C long range scalar correlation spectrum, obtained with a gs-HMBC pulse sequence, eight scans, 2 s as repetition time, 1024 increments in ^{13}C dimension and a delay 1/2J = 3.12 ms corresponding to mean $^1J_{C—H}$ = 160 Hz. ^1H and ^{13}C $\{^1H\}$ T_1 measurements involved a classical inversion-recovery sequence, with ^1H decoupling in the case of ^{13}C. We adopted a 10 s repetition time with two scans for ^1H and 5 s with 1024 scans for ^{13}C.

2.5. Electron density modeling

All calculations were made using the homemade PACHA software [34,35]. This software was designed for retrieving a partial charge distribution from the molecular or crystalline structure without the introduction of empirical parameters. Briefly stated, these charges are recovered after application of the electronegativity equalization principle that is known to have a firm quantum-mechanical basis and a deep thermodynamic significance as a measure of the electronic chemical potential. The transformation of a set of atomic coordinates into a partial charges distribution is performed using an atomic parameterization resting on two non-empirical parameters per atom: an electronic chemical potential measured by a spectroscopic electronegativity (Allen's scale) and an atomic radius measured by the most diffuse principal maxima in the radial distribution function $r^2\psi^2(r)$, computed using relativistic wavefunction solutions of the Dirac equations. Interested readers should refer to the original papers for more details [34,35]. In the present case, the original CIF file cannot be used as such, owing to missing H-atom coordinates and to large uncertainties in the position of H-atoms and/or solvent molecules (here dioxane and ethanol). Consequently, in order to get electronic densities that reflects the averaged topology observed in solution and not the various metrical errors coming from the crystal structure determination in the solid state, the structure has been standardized in the following way.

All bonds involving H-atoms were first scaled to some standard values (see [36] for a compilation). In this study, O—H, Car—H, C—H bonds in methylene and C—H bonds in methyl groups have all been set equal to 97, 108, 109 and 106 pm respectively. Similarly all H—C—H bond angles in methylene and methyl groups have been set equal to their ideal tetrahedral value (110°). For methylene groups, standard torsion angles ±120° were assumed, whereas for the methyl group, one torsion angle was arbitrarily varied, the two other ones being fixed at ±120°. For the hydrogen bridge between Hbhmpc and H_2bhmpc ligands (see Fig. 2), the H41—O3—C7—O6 torsion angle was fixed to 0° to avoid divergence in the

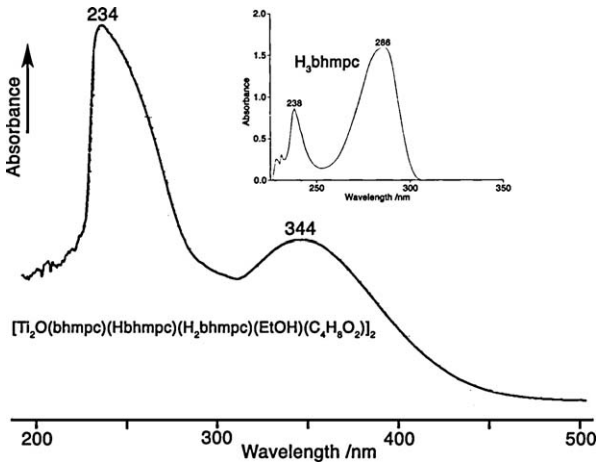

Fig. 2. U.V.-Vis. spectra for the free ligand H_3bhmpc and for the crystals $\{[Ti_2O(bhmpc)(Hbhmpc)(H_2bhmpc)].C_4H_8O_2.EtOH\}_2$ dissolved in $CHCl_3$.

charge distribution. For the three remaining hydrogen bonds the corresponding torsion angle was arbitrarily varied.

The atomic coordinates for dioxane and ethanol were recomputed starting from one oxygen atom (labeled O11 for dioxane and O13 for ethanol in the CIF file) using 143 and 153 pm for C—O and C—C bond lengths. Among the 10 and four angles needed to fix in space the dioxane and ethanol molecules, respectively, (3 + 3) were arbitrarily varied, the other ones (7 for dioxane and 1 for ethanol) being fixed at 110° (O—C—C and C—O—C bond angles) and ±60° (torsion angles). This procedure allows one to conserve the overall ''chair shape'' identified for the dioxane molecule in the original X-ray data file and avoids the large metrical distortions observed in this CIF file.

After this parameterization, there remained 13 arbitrary angles associated to the mobile part of the complex that are —CH_2—OH and —CH_3 groups or dioxane and ethanol orientation in the two divergent cavities. A reasonable structural model for describing the solution behavior is then derived by applying a two-step non-empirical energy minimization technique. In a first step involving the 13 variable angles, we have looked for the geometry corresponding to a minimum in steric energy by using short-range repulsive potentials derived from the Gordon–Kim electron gas model [37]. These non-empirical potentials are known to correlate extremely well with experimental van der Waals or non-bonded radii and were successfully used in a previous work [38]. In a second step, all H-atoms positions (7 arbitrary angles) were deduced after minimization of the electrostatic lattice energy using the non-empirical PACHA scheme [34,35,39]. It was found to be very close to the experimental one concerning the O-atom and C-atom coordinates and now contains all H-atoms in their most favorable position (both from a steric and electrostatic viewpoint) with ideal bond lengths and almost perfect tetrahedral bond angles.

2.6. Correlation of electron densities with NMR shifts

Previous studies have shown that the electron densities retrieved from the PACHA software were very useful for interpretation of chemical shifts variations [40–46]. Referring to an absolute scale (σ_{ref} = 185.4 ppm) [47], the chemical shift δ of a ^{13}C nucleus bearing a partial charge q and submitted to an average excitation energy ΔE with an electronic population unbalance in p-orbitals P_u may be expressed as [45,46]:

$$\delta = \sigma_{ref} - \sigma_{dia}(q) + 966 \cdot \frac{\langle (a_0/r)^3 \rangle_{2p}}{\Delta E} \cdot P_u \qquad (1)$$

$$P_u = (P_{xx} + P_{yy} + P_{zz}) - \frac{1}{2}(P_{xx} \cdot P_{yy} + P_{yy} \cdot P_{zz} + P_{zz} \cdot P_{xx}) + \frac{1}{2}(P_{xy} \cdot P_{yx} + P_{xz} \cdot P_{zx} + P_{yz} \cdot P_{zy})$$

In this relationship, the diamagnetic contribution $\sigma_{dia}(q)$ may be evaluated from Hartree–Fock–Slater wave functions using the procedure of Saxena and Narasimhan [48] while the effect of partial charge q on the electron–nucleus distance r averaged over 2p-orbitals may be modeled as $< (a_0/r)^3 >_{2p} = R^\circ \cdot (1 - f \cdot q)$, where R° = 1.23 a.u. is the value applying to a free neutral carbon atom [49] and f a dimensionless factor close to unity. Molecular orbital theory is usually applied for recovering the charge distribution and bond order matrix P_{ij} ($i, j = x, y$ or z) governing the P_u-term [50,51] as well as the average excitation energy ΔE. These treatments, being in any case very approximate, we prefer to assume equal sharing of the electronic density among the three p-orbitals: $P_{xx} = P_{yy} = P_{zz} = P$, $P_{xy} = P_{yx} = P_{xz} = P_{zx} = P_{yz} = P_{xy} = 0$. With P_{ss}, the population of the carbon 2s-orbital charge conservation leads to $P_{ss} + 3P = 4 - q$, i.e. $P = (1 - q/3)$ if $P_{ss} \approx 1$, leading to $P_u = 3/2(1 - q^2/9)$. The average excitation energy ΔE was evaluated by inversion of Eq. (1) using an average chemical shift computed from a set of NMR resonances characterized by the same first coordination sphere and from the corresponding averaged partial

charges and diamagnetic shifts. Values less than 1 eV or much larger than 20 eV usually indicate wrong scaling in the charge dependence of the $<(a_0/r)^3>_{2p} = R^{\circ}\cdot(1 - f\cdot q)$ term.

2.7. Thermodynamic modelization

In addition of bringing considerable help in the spectroscopic characterization of sol–gel precursors and in the quantification of ionic characters for any kind of molecular interactions, the PACHA approach may also be used to discuss chemical reactions from a thermodynamic viewpoint. This was already the case with the original partial charge model developed in collaboration with J. Livage [20–23], but with the ability of taking now into account the detailed molecular structures of the precursors it is now possible to perform a fully quantitative treatment of both enthalpic and entropic contributions. As far as enthalpy is concerned, PACHA relies onto the Hellman–Feynman theorem allowing one to introduce a unique partition of the molecular internal energy into a SE-term accounting for inter-atomic contributions, and a F-term accounting for intra-atomic electronic contributions independent of nuclear coordinates (see [35] for a rigorous quantum-mechanical treatment). Assuming that the variations of the F-term are well accounted by the choice of the Allen's absolute electronegativity scale used to derive equilibrium partial charges distributions and using the spherical charge approximation, it is possible to identify the SE-term with the internal energy U of the system. Using the common assumption that $U \approx H$ for condensed phases, it comes that the enthalpy variation ΔH should scale like the ΔSE variation.

Concerning entropy variations PACHA is able to estimate rotational entropies S_{rot} at temperature T for a given molecular structure by computing its three principal moments of inertia (I_A, I_B, I_C) and assuming that all rotational energetic levels are accessible at room temperature, leading to [52]:

$$S_{rot} = R\cdot\ln\left[\frac{\left(k_B T\cdot e\right)^{3/2}}{\sigma\cdot\hbar^3}\cdot\sqrt{8\pi\cdot I_A\cdot I_B\cdot I_C}\right] \qquad (2)$$

In this relation, k_B is Boltzman's, e is Neper's constant, $\hbar$ is reduced Planck's constant, R is the ideal gas constant and σ is the number of indistinguishable orientations of the molecule (symmetry number equal to the order of the rotational sub-group of the molecular point-group). If such an approximation is obviously not justified for very small molecules, it should work quite well for sol–gel precursors that are precisely not small molecules. It is worth stressing that (2) applies only to rigid rotators having no flexible parts. For molecules having flexible parts, such as freely rotating methyl groups, for instance, an additional contribution of about 15 J.mol^{-1}.K^{-1} per methyl group should be added to (2) [53]. Besides free rotation around its three principal inertia axes, PACHA also consider the experimental IR and Raman frequencies ν_i associated to the 3N-5 (linear molecule) or 3N-6 (non-linear molecules) vibration modes using the following computational scheme [53]:

$$S_{vib} = R\cdot\sum_{i=1}^{3N-5or6}\left[\frac{h\nu_i/k_B T}{\exp(h\nu_i/k_B T)-1} - \ln\left(1-\exp\left\{-\frac{h\nu_i}{k_B T}\right\}\right)\right] \qquad (3)$$

Finally, besides this internal entropy $S_{int} = S_{rot} + S_{vib}$, PACHA also computes a standard partial molar entropy (molar scale, SI units) S° using a classical partition function derived by Powell and Latimer [54]:

$$S^{\circ} = S_{int} + R\cdot\ln V_S + \frac{3R}{2}\cdot\ln T + \frac{3R}{2}\cdot\ln M + R\cdot\ln\left(\frac{2\pi\cdot k_B\cdot e^{5/3}\cdot 10^{-5}}{{N_A}^{5/3}\cdot h^2}\right)^{3/2} \qquad (4)$$

In this relation, $S_{int} = S_{rot} + S_{vib}$ is the internal contribution, V_S is the molar volume of the solvent expressed in L.mol^{-1}, M is the molar weight of the solute expressed in g.mol^{-1}, N_A is Avogadro's number, h is the Planck's constant while e, R and k_B have the same meaning as in Eq. (2). The rotational entropy of (**1**) and H_3bhmpc have thus been estimated from the knowledge of their crystalline structure ([33] and CSD code MUGNAD respectively) assuming free rotation of the methyl group and from the IR/Raman data given in Tables 1 and 2. Two geometries were considered for H_3bhmpc: one with two intramolecular H-bonds after SE-minimization and one with intermolecular H-bonds observed in the solid-state structure. Vibrational entropy of H_3bhmpc has been computed using the experimental IR and Raman spectra available on Sigma–Aldrich's web site. Structural models for other compounds have been generated by minimization of repulsive energy using short-range repulsive potentials derived from the Gordon–Kim electron gas model [37] and assuming perfectly tetrahedral bond angles with C—C distances of 153 pm, C—O distances of 142 pm, C—H distances of 108 pm and O—H distances of 97 pm. Ideal structural models have been thus generated using the above standard structural parameters for

Table 1
Attribution of the IR spectrum shown in Fig. 1. Greek letters ν,δ,π,φ,ρ^w and ρ^r refer to stretching, scissoring, out-of-plane deformation, aromatic ring breathing, wagging and rocking vibrations respectively. Harmonic vibrations and ring breathing of 1,4-dioxane are noted "harm" and "ring" respectively.

Vibration	H_3bhmpc	1,4-dioxane	Complex	$\Delta\nu_1$	$\Delta\nu_2$
$\nu_{O—H}$	3396, 3313, 3173	-	3440 (400)	+44	-
$\nu_{Ph—H}$	-	-	3003	New	−2
$\nu^a_{CH2(O)}$	2962	2964	2962	0	−2
ν^a_{CH3}	2925	-	2948	+23	-
$\nu^a_{CH2(C)}$	2911	2914	2911	0	−3
$\nu^s_{CH2(O)}$	2869	2889	2883	+14	−6
$\nu^s_{CH2(C)}$	2854	2856	2853	+1	−3
Harm.	-	2754	2738	-	−16
Harm.	-	2694	2685	-	−9
$\nu^{ar}_{C—C}$	1606	-	1636	+30	-
$\nu^{ar}_{C—C}$	-	-	1603, 1586	New	-
δ^a_{CH3}	1485	-	1473	−12	-
$\delta_{CH2(O)}$	1453	1454	-	-	-
$\delta_{CH2(C)}$	1447	1446	1444	−3	+2
δ^S_{CH3}	1418	-	1418	0	-
$\pi_{CH2(O)}$	1372	1366	1397	+25	+31
ρ^w_{CH2}	1320	1324	1323	+3	+4
$\pi_{CH2(C)}$	1266	1289	-	-	-
Ring	-	1254	1256	-	+2
$\delta_{C—O—H}$	1247	-	1244	-3	-
$\nu^{ar}_{C—O}$	1206	-	1219	+13	-
$\nu^a_{C—O}$	1155	-	1160	+5	-
$\nu^a_{C—O}$	-	1122	1119	-	−3
$\nu^S_{C—O}$	1063	1083	1078	+15	−5
$\nu_{C—O(Ti)}$	-	-	1046	New	-
$\delta_{Ph—H}$	1016	-	1016	0	-
$\phi_{C—C}$	1006,619,593,560	-	-,633,-,578	+14...+18	-
Ring	-	1049,889,874	1046,889,871	-	0...−3
π_{PhH}	997,976,867,662	-	998,-,862,673	−5...+11	-
$\nu_{Ph—C}$	960	-	960	0	-
μ_3-OTi	-	-	840,826	New	-
$\delta_{Ti—O—C}$	-	-	703	New	-
ρ^r_{CH2}	766,746,740	-	774,754,-	+8	-
μ_3-OTi	-	-	502,458	New	-

1,4-dioxane ($V_S = 0.0853$ L.mol^{-1}), EtOH and ^{i}PrOH with free rotation of methyl groups, while the best *ab initio* molecular geometry [55] has been considered for the water molecule. Vibrational entropies of 1,4-dioxane, EtOH and ^{i}PrOH have been computed using the experimental IR and Raman spectra available at the SDBS database [56]. Concerning titanium alkoxides precursors, the $\{Ti_4O_{16}\}$ core of $[Ti_4(OMe)_{16}]$ [57] has been used for building a molecular model of tetrameric $[Ti_4(OEt)_{16}]$ known to exist in the solid state [58], while XANES/EXAFS data [59] have been used for trimeric $[Ti_3(OEt)_{12}]$. Owing to the unknown status of free rotation of the methyl groups in these structures, they were all considered as rigid rotators with no flexible parts. For monomeric $[Ti(OPr^i)_4]$, it was found that the SE-energy was highly sensitive to the choice of the Ti—O distance. Using the 1.77 Å Ti—O distance measured on pure titanium isopropoxide [59] leads to SE = −4548 kJ.mol^{-1}, a much too low value leading to abnormally highly endothermic reactions even with water. Using the 1.82 ± 0.02 Å Ti—O distance measured also by EXAFS on titanium isopropoxide dissolved in toluene [60] leads to SE = −3732 ± 234 kJ.mol^{-1}, a value more compatible with known $Ti(OPr^i)_4$ chemistry. For this study performed in dioxane/alcohol mixtures where H-bonding may readily occur, the upper uncertainty limit (Ti—O = 1.84 Å) has been selected accounting for a possible additional extension due to H-bonding interactions that are absent in toluene. As in the case of titanium ethoxide, $Ti(OPr^i)_4$ has been considered as a rigid rotator with no flexible parts (fully hindered rotation of methyl groups). Vibrational entropies for these titanium(IV) alkoxides have been computed using their experimental IR and

Table 2
Attribution of the Raman spectrum shown in Fig. 2. Greek letters ν,δ,π,ϕ and ρ^w and refer to stretching, scissoring, out-of-plane deformation, aromatic ring breathing, and wagging vibrations respectively. Ring breathing of 1,4-dioxane is noted "ring".

Vibration	H_3bhmpc	1,4-dioxane	Complex	$\Delta\nu_1$	$\Delta\nu_2$
$\nu_{Ph—H}$	3012	-	2997	−15	-
$\nu^a_{CH2(O)}$	2955	2967	2962	+7	−5
ν^a_{CH3}	2921	-	2930	+9	-
$\nu^a_{CH2(C)}$	2912	-	-	-	-
$\nu^s_{CH2(O)}$	2879	2890	-	-	-
$\nu^s_{CH2(C)}$	-	2858	-	-	-
$\nu^{ar}_{C—C}$	1618	-	1644	+26	-
$\nu^{ar}_{C—C}$	1606	-	-	-	-
$\nu^{ar}_{C—C}$	-	-	1504	New	-
δ^a_{CH3}	1485	-	1483	−2	-
$\delta_{CH2(O)}$	1471	1457	-	-	-
$\delta_{CH2(C)}$	1446	1443	-	-	-
δ^S_{CH3}	1380	-	1378	−2	-
ρ^w_{CH2}	1346	1331	1327	−19	−4
π_{CH2}	1318	1304	1296	−22	−8
π_{CH2}	-	-	1281	New	-
Ring	-	1215	-	-	-
$\nu_{C—O(Ti)}$	-	-	1242	New	-
$\nu^{ar}_{Ph—C}$	1198	-	1221	+23	-
$\nu_{C—C}$	1160	-	1162	+2	-
$\delta_{Ph—H}$	1020	-	-	-	-
Ring	-	1014	-	-	-
$\phi_{C—C}$	995	-	996	+1	-
$\nu_{Ph—C}$	965	-	949	−16	-
Ring/μ_3-O	-	835	835	-	0
ν^{ar}_{cycle}	795	-	-	-	-
ν^{ar}_{cycle}	671	-	-	-	-
$\nu_{Ti—O}$	-	-	628,597	New	-
$\phi_{C—C}$	577	-	585	+8	-
$\phi_{C—C}$	519	-	532	+13	-
$\delta_{C—C}$	474	485	489	+15	+4
$\nu_{Ti—O}$	-	-	448	New	-
$\phi_{C—C}$, $\delta_{C—C}$	414	432	432	+18	0
$\delta_{C—C}$	380	-	390	+10	-
$\delta_{C—C}$	357	-	346	−11	-

Raman spectra available on Sigma–Aldrich's web site [61] (Table 3).

3. Results

3.1. U.V.-vis. spectroscopy

One of the most remarkable features of the complex is its deep orange color, a not so common situation for Ti^{IV}-based complexes. Fig. 2 compares the U.V.-Vis. spectra of the complex with that of the free ligand. The high energy band of the free ligand assigned to $\pi\rightarrow\pi^*$ transitions within the aromatic ring is characterized by $\lambda_{max} = 238$ nm ($\varepsilon = 1200$) and undergoes a slight hypsochromic shift, $\lambda_{max} = 234$ nm, associated to a significant intensity increase ($\varepsilon = 18700$) after binding to Ti(IV)-centers. The low energy band of the free ligand assigned to $n\rightarrow\pi^*$ transitions between O-atom lone pairs and the anti-bonding orbitals of the aromatic ring is characterized by $\lambda_{max} = 286$ nm ($\varepsilon = 2300$) and

Table 3
Partial charges distribution calculated from crystal data, experimental chemical shifts and NMR assignment to crystal sites for hydrogen atoms contained in (**1**). See Fig. 8 for XRD data libeling and Figs. 9–11 for NMR signals labeling.

Chemical type	XRD label (neighbors)	Charge q	Shift/ppm	NMR label
Dioxane $C_4\underline{H}_8O_2$	**H31**(C28)	+0.0251	3.664	
	H30(C28)	+0.0422	3.664	
	H35(C30)	+0.0462	3.664	
	H32(C31)	+0.0511	3.664	
	H34(C30)	+0.0550	3.664	
	H28(C29)	+0.0550	3.664	
	H33(C31)	+0.0585	3.664	
	H29(C29)	+0.0654	3.664	
$C\underline{H}_3CH_2OH$	**H40**(C33)	+0.0435	1.146	
$C\underline{H}_3CH_2OH$	**H38**(C33)	+0.0504	1.146	
$CH_3C\underline{H}_2OH$	**H37**(C32)	+0.0507	3.615	
$C\underline{H}_3CH_2OH$	**H39**(C33)	+0.0638	1.146	
$CH_3C\underline{H}_2OH$	**H36**(C32)	+0.0649	3.615	
Methyle $C\underline{H}_3$	**H22**(C17)	+0.0483	2.197	*H2*
	H24(C17)	+0.0487	2.197	*H2*
	H23(C17)	+0.0579	2.197	*H2*
	H19(C8)	+0.0506	2.226	*H3*
	H21(C8)	+0.0537	2.226	*H3*
	H20(C8)	+0.0574	2.226	*H3*
	H25(C26)	+0.0519	2.166	*H1*
	H26(C26)	+0.0534	2.166	*H1*
	H27(C26)	+0.0669	2.166	*H1*
Methylene $C\underline{H}_2$	**H17**(C19)	+0.0191	5.608	*H12*
	H18(C19)	+0.0502	4.868	*H9*
	H15(C27)	+0.0299	5.909	*H15*
	H16(C27)	+0.0611	4.805	*H7*
	H7(C7)	+0.0301	5.826	*H14*
	H8(C7)	+0.0623	5.672	*H13*
	H14(C10)	+0.0308	5.338	*H11*
	H13(C10)	+0.0385	4.818	*H8*
	H10(C9)	+0.0519	4.744	*H6*
	H9(C9)	+0.0534	4.172	*H5*
	H12(C18)	+0.0538	4.050	*H4*
	H11(C18)	+0.0618	5.035	*H10*
Aromatic C—$\underline{H}$	**H5**(C21)	+0.0493	6.709	*H16*
	H1(C3)	+0.0516	6.947	*H21*
	H4(C14)	+0.0523	6.929	*H20*
	H2(C5)	+0.0548	6.788	*H17*
	H6(C23)	+0.0558	6.799	*H18*
	H3(C12)	+0.0596	6.823	*H19*
$ArCH_2(O\underline{H})$—Ti	**H41**(O3)	+0.1879	-	
$ArCH_2(O\underline{H})$...EtOH	**H42**(O4)	+0.1882	-	
$ArCH_2(O\underline{H})...O_2C_4H_8$	**H43**(O6)	+0.2016	-	
$CH_3CH_2O\underline{H}$	**H44**(O13)	+0.2085	-	

undergoes a large bathochromic shift, λ_{max} = 344 nm, with a significant intensity increase (ε = 8000) after binding to Ti(IV)-centers. This last band is responsible for the orange-color of the complex owing to its considerable width (*ca.* 100 nm at half-height) that may be assigned to charge transfers between the lone pairs of phenolic O-atoms and the empty 3d-orbitals on Ti-atoms.

3.2. IR spectroscopy

Attribution of the spectrum (Fig. 3) has been made (Table 1) by comparison with the IR spectra of the free ligand H_3bhmpc [61] and of 1,4-dioxane [62]. Upon complexation, the three $\nu_{O—H}$ bands found in the H_3bhmpc ligand are replaced by a single large band centered at 3440 cm^{-1} ($\Delta\nu_{1/2}$ = 400 cm^{-1}). It is thus not possible to differentiate between the three kinds of intramolecular H-bonds existing in the crystal. Complexation has also the effect of rendering visible $\nu^{ar}_{C—H}$ and $\nu^{ar}_{C—C}$ vibrations that are not observed in the free H_3bhmpc ligand. For the other bands, the global effect of complexation is an increase in frequency of at most 30 cm^{-1} except for δ^{a}_{CH3}, δ_{CH2}, $\delta_{C—O—H}$ vibrations and one $\pi_{Ph—H}$ component showing a decrease in frequency of at most –12 cm^{-1}. A few bands ν^{a}_{CH2}, δ^{S}_{CH3}, $\delta_{Ph—H}$, $\nu_{Ph—C}$ are also observed at the same frequency in the free ligand or in the complex. On the other hand, it is observed that encapsulation of 1,4-dioxane within the two cavities has the global effect of decreasing vibrations frequencies by at most –16 cm^{-1} except for $\delta_{CH2(C)}$, $\pi_{CH2(O)}$, ρ^{w}_{CH2} and one type of ring breathing vibrations showing small increase in frequency except for the $\pi_{CH2(O)}$ vibration that appears to be strongly affected. This detailed attribution has allowed detection of the vibration bands associated to the formation of Ti—O bonds. The frequency found for the $\nu_{C—O(Ti)}$ band is within the expected 1000–1170 cm^{-1} range for Ti—O—C bonds while that proposed for the μ_3-oxo bridge are close to what is observed in the rutile structure showing similar bridges: 811 cm^{-1} (A_{2u}, longitudinal), 806 cm^{-1} (A_{2u}, longitudinal), 500 cm^{-1} (E_u, transverse) and 458 cm^{-1} (E_u, longitudinal) [63]. The assignment of the 703 cm^{-1} band with $\delta_{Ti—O—C}$ is tentative and should not be considered as firmly established.

3.3. Raman spectroscopy

Attribution of the spectrum (Fig. 4) has been made (Table 2) by comparison with the Raman spectra of the free ligand H_3bhmpc [61] and of 1,4-dioxane [64]. The spectrum is dominated by the aromatic doublet at (1644, 1504) cm^{-1} and by the breathing of the dioxane ring at 835 cm^{-1}. As already observed in the IR spectrum, the global effect of complexation is an increase in frequency

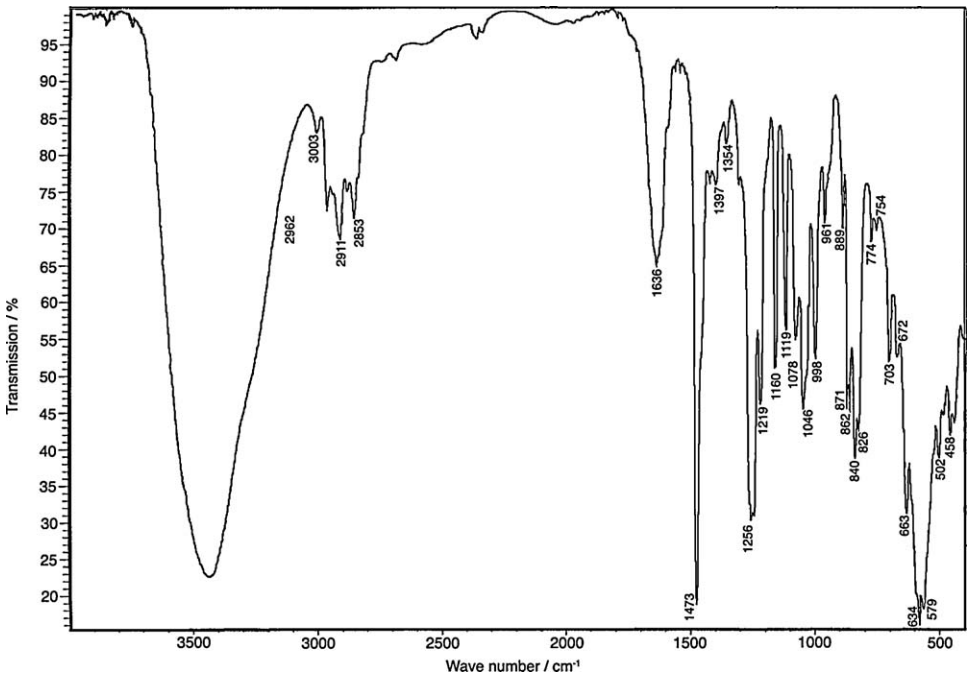

Fig. 3. Infrared spectrum of $\{[Ti_2O(bhmpc)(Hbhmpc)(H_2bhmpc)].C_4H_8O_2\}_2$ crystals dispersed in KBr pellets. See Table 1 for the assignment.

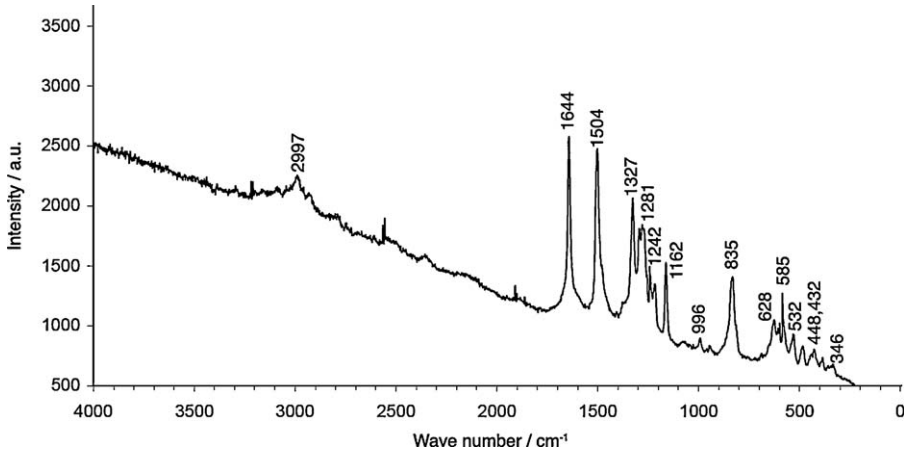

Fig. 4. Raman spectrum of $\{[Ti_2O(bhmpc)(Hbhmpc)(H_2bhmpc)].C_4H_8O_2\}_2$ microcrystalline powders after deposition on a glass wafer. See Table 2 for the assignment.

of at most 26 cm^{-1} except for δ^{a}_{CH3}, δ^{S}_{CH3}, ρ^{w}_{CH2}, π_{CH2} vibrations and one $\nu_{C—C}$ component showing rather a decrease in frequency of at most –22 cm^{-1}. It is also again observed that encapsulation of 1,4-dioxane within the two cavities has the global effect of decreasing vibration frequencies of at most –8 cm^{-1} except for one $\delta_{C—C}$ component showing a slight increase in frequency and two vibrations (ring breathing and $\delta_{C—C}$) being unaffected. This detailed attribution has allowed detection of vibration bands associated to the formation of Ti—O bonds. The frequency found for the $\nu_{C—O(Ti)}$ band is slightly higher than the 1160–1180 cm^{-1} range for observed for aliphatic Ti—O—C bonds [65]. This increase in frequency may well reflect the fact that we are dealing here with an aryloxide and not with an alkoxide. The attribution proposed for the $\nu_{Ti—O}$ and μ_3-oxo bonds is in agreement with what is observed in the rutile structure showing similar bridges: 826 cm^{-1} (B_{2g}), 612 cm^{-1} (A_{1g}) and 447 cm^{-1} (E_g) [63] or in the Raman spectra of titanium alkoxides [65].

3.4. ^{17}O NMR spectroscopy

Fig. 5 shows the 44.2 MHz ^{17}O NMR spectrum of complex (**1**) dissolved in $CDCl_3$. As expected, only one signal is observed at 455 ppm falling within the 450–650 ppm range expected for μ_3-OTi_3 bridges [31–32].

3.5. ^{13}C solid state CPMAS NMR

Fig. 6 shows the different ^{13}C CPMAS NMR spectra recorded at 75 or 125 MHz for different crystals obtained after mixing in 1,4-dioxane, H_3bhmpc and $Ti(OR)_4$ using R = Et (spectra 1-4) or R = Pr^i, Bu^n (spectrum 5). According to the two single-crystal X-ray structures available for the R = Et compounds [33], three signals corresponding to bhmpc, Hbhmpc and H_2bhmpc ligands are expected for phenolic **C**—O(Ti) and Ph—**C**H_3 sites in the as synthesized crystals, while six signals should be obtained after recrystallization in $CHCl_3$ owing to the existence of two non-equivalents complexes in the unit-cell of this last compound. Spectra 1, 2 and 4 are in good agreement with this analysis. The two spectra recorded on samples 1 and 2 illustrate the effect of drying the crystals at room temperature under ambient atmosphere. In the phenolic **C**—O(Ti) region (left of Fig. 6), drying essentially affects the chemical shift of the central resonance which moves from 157.0 ppm (sample 1) to 156.5 ppm (sample 2), the two outer resonances at 159.4 and 153.7 ppm being almost unaffected (159.6 et 153.7 ppm in sample 2). In the methyl region (right of Fig. 6), the number of signals changes from 4 to 3 with a change in chemical shifts for all resonances, reflecting the fact that ethanol molecules are no more present in the structure (while dioxane is still trapped as can be seen on Fig. 7). The spectrum of sample 3 in Fig. 6 points out the existence of at least two polymorphs in the as synthesized crystalline powders of the R = Et system. A pure single phase (1) is usually produced but, in spite of identical working conditions, obtaining a mixture similar to sample 3 is not rare. As will be discussed below, this mixture appears to contain two polymorphs. Spectrum 3 can actually be fitted as a sum of a spectrum identical to 1 (major component) and a second spectrum which appears to be identical to 5. Spectrum 5 is the reproducible signature of orange crystalline powders obtained when either $Ti(OPr^i)_4$ or $Ti(OBu^n)_4$ are used as

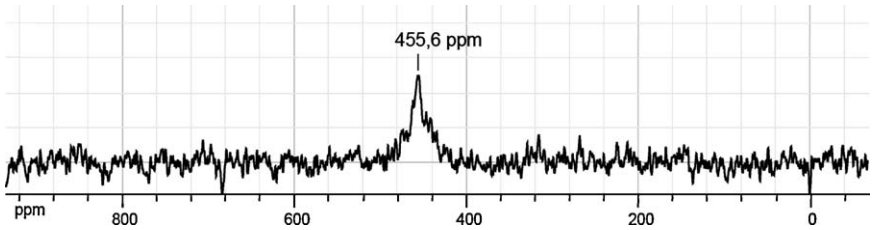

Fig. 5. Natural abundance ^{17}O NMR spectrum recorded at 44.2 MHz after partial dissolution of {[Ti_2O(bhmpc)(Hbhmpc)(H_2bhmpc)].$C_4H_8O_2$.EtOH}$_2$ crystals in $CDCl_3$.

sources of titanium instead of $Ti(OEt)_4$. In these cases, no alcohol or alkoxy signals are present on spectra that are the same for both sources of titanium, but in each case 1,4-dioxane molecules are detected. In the phenolic **C**—O(Ti) region of the spectrum, six components can be identified at 159.7, 159.5, 157.1, 156.9, 153.0 and 152.7 ppm. This can be compared to the case of sample 4, obtained by recrystallization in $CHCl_3$ for which six signals are also found, shifted, at 159.7, 159.4, 159.0, 158.4, 153.5 and 153.0 ppm. This similarity suggests a single-phase composition for samples giving rise to spectrum #5, corresponding to a polymorph with two non-equivalent molecules in the unit-cell as was observed with the recrystallized sample 4. Unfortunately all attempts to determine this new crystalline structure suggested by ^{13}C CPMAS measurements have failed owing to the very small size of the crystals, not suitable for a single-crystal X-ray study. Fig. 7 shows the two other regions of interest in these ^{13}C CPMAS spectra that are either too complex to be analyzed in details (aromatic carbons zone at the left) or sometimes showing a bad resolution (methylene zone at the right for spectra 3 to 5). Despite this lack of resolution, it is worth noticing the absence of ethanol

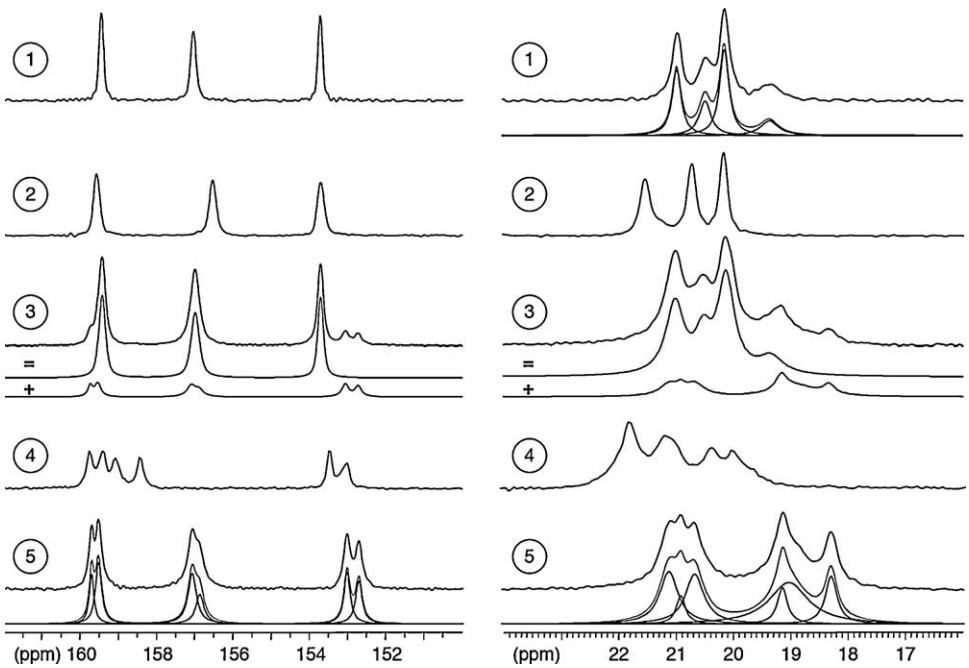

Fig. 6. ^{13}C CPMAS NMR spectra recorded at 75 MHz (1,2) or 125 MHz (3-5), (see experimental section for details), for different crystals obtained after mixing in 1,4-dioxane, H_3bhmpc and $Ti(OR)_4$ using R = Et (spectra 1-4) or $R = Pr^i$, Bu^n (spectrum 5). Spectra 1, 3 and 5 have been recorded on as synthesized crystals. Spectrum 4 corresponds to crystals obtained after recrystallization in $CHCl_3$ (starting from spectrum 1 - crystals). Spectrum 2 is obtained after drying spectrum 1 - crystals. Phenolic **C**—O region is shown at the left while Ph—**C**H_3 is displayed at the right. The decomposition of some parts of spectra, obtained with Dmfit software analysis, is shown (dark grey: individual components; light grey: simulated sum-spectrum). See D. Massiot, F. Fayon, M. Capron, I. King, S. Le Calvé, B. Alonso, J-O. Durand, B. Bujoli, Z. Gan, G. Hoatson, Magn. Reson. Chem., 40 (2002) 70 for details.

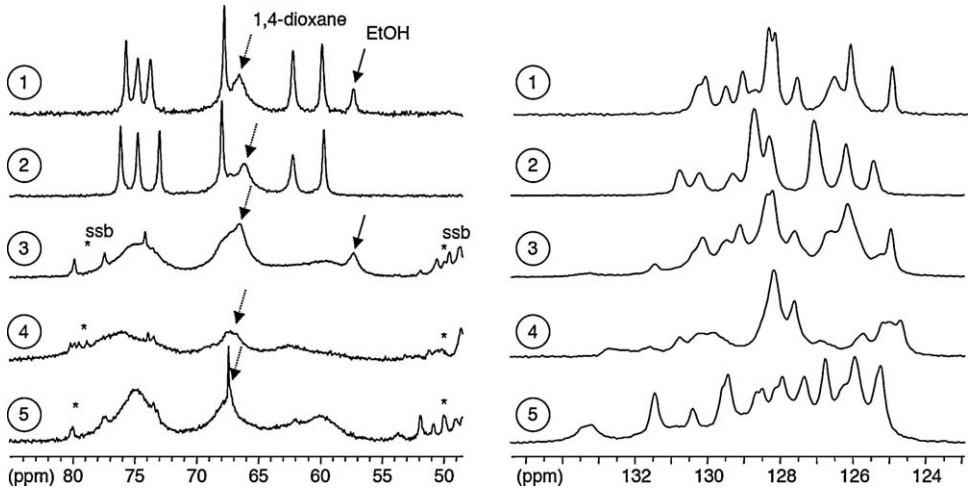

Fig. 7. ^{13}C CPMAS NMR spectra recorded at 75 or 125 MHz for the same crystalline powders analyzed in Fig. 6. Aromatic carbon region is shown at the left while methylene region is displayed at the right. Stars denote groups of spinning sidebands (ν_R = 10 kHz for 1,2 and ν_R = 13 kHz for 3-5).

signals in samples 2, 4 and 5 in good agreement with the above discussion. It is also worth noting that 1,4-dioxane is detected in all cases as a large signal at 66–67 ppm. For sample 4, identifying the signal due to included $CHCl_3$ molecules on the ^{13}C CPMAS spectrum is not straightforward because of superimposed large signals but the presence of these molecules could be clearly evidenced by comparison with $^{13}C\{^1H\}$ MAS spectrum and on the ^1H MAS spectrum (not shown).

3.6. *^1H and ^{13}C solution NMR spectroscopy*

It was observed that all samples studied by ^{13}C CPMAS NMR gave rise to exactly the same ^1H or ^{13}C spectra after dissolution in $CDCl_3$. This shows that if the nature of the R group used for the synthesis has a subtle effect upon the stacking of such molecules in the solid state, it plays absolutely no role in the building of the molecular unit in solution. Consequently, three different kinds of signals coming from aromatic ligands: bhmpc, Hbhmpc and H_2bhmpc are expected if the centrosymmetric structure of the complex is conserved upon dissolution. For discussion we have labeled each peak on ^1H and ^{13}C spectra starting from low frequencies and ignoring solvent molecules. Fig. 8 shows the numbering scheme derived from X-ray crystallography, while Fig. 9 gives the final ^1H and ^{13}C NMR assignment.

Fig. 10 shows the ^1H spectrum of a sample of (**1**) dissolved in $CDCl_3$, (5 mg/0.6 mL). Dioxane and ethanol are readily identified by a singlet at 3.66 ppm (O—C**H**$_2$—C**H**$_2$—O), a quadruplet at 3.61 ppm (CH_3—C**H**$_2$—OH) and a triplet at 1.15 ppm (C**H**$_3$—CH_2—OH) respectively. Some free H_3bhmpc is also detected by the occurrence of three signals at 6.62 ppm (aromatic C—**H**), 4.45 ppm (O—C**H**$_2$—Ar—) and 2.19 ppm (—Ar—C**H**$_3$). Other signals may be attributed to the three different kinds of ligands. No signal is detected from any hydroxy proton, clearly due to exchange processes. The methyl groups of the cresol moiety lead to three well-resolved signals (1:1:1) between 2.1 and 2.3 ppm. Between 4 and 6 ppm, 12 doublets of equal integral are observed showing the existence of six inequivalent

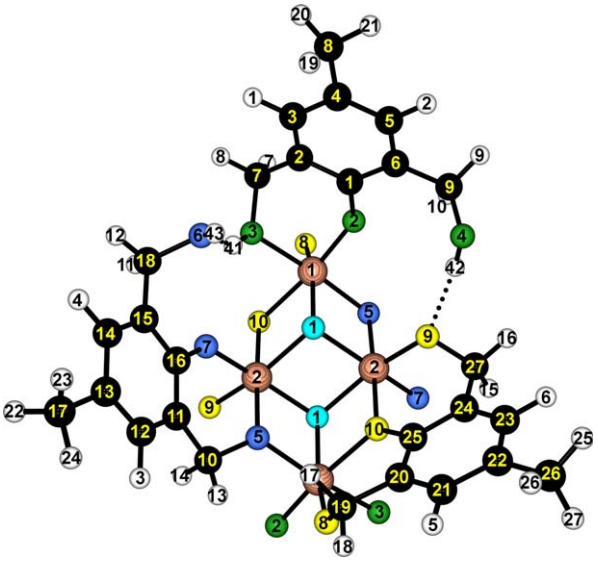

Fig. 8. Atomic labels for (**1**) in the optimized X-ray crystal structure reported as a CIF file in the supplementary material. See Tables 7 and 8 for the complete charge distribution and NMR assignments. Only one ligand of each type is represented.

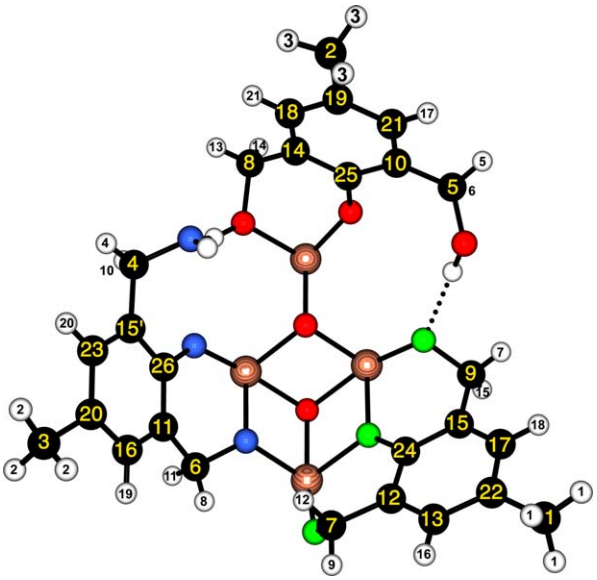

Fig. 9. Atomic labels for (**1**) resulting from the assignment of NMR ^{1}H and ^{13}C NMR signals to molecular sites. Only one ligand of each type is represented.

methylene groups, each bearing two inequivalent protons. Four measured ^{2}J values are significantly different (11.1, 11.8, 13.55, 14.5 Hz) and lead to pair some signals corresponding to different CH_2 groups, respectively, (*H5,H6*), (*H4,H10*), (*H13,H14*) and (*H9,H12*). ^{2}J values measured for the doublets *H7, H8, H11* and *H15* are too close and distributed (13.33, 13.38, 13.31, 13.25) to show pairs unambiguously. According to the second order coupling figures, one can nevertheless pair ^{1}H signals the following way: (*H11,H7 or H8*) and (*H15, H7 or H8*). Finally, between 6.7 and 7 ppm, six doublets ($^{4}J \sim 1.6$ Hz) of equal integral are observed corresponding to the two aromatic protons of the three kind of ligands. Detailed ^{1}H chemical shift values can be found Table 1.

Fig. 11 shows the ^{13}C {^{1}H} spectrum on the same sample. As before, dioxane and ethanol are detected by three signals at 67.1 ppm (O—**C**H_2—**C**H_2—O), 58.4 ppm (CH_3—**C**H_2—OH) and 18.3 ppm (**C**H_3—CH_2—OH). Signals attributed to the complex are: three signals observed at 20–21 ppm (—Ar—**C**H_3), six signals at 60–75 ppm (O—**C**H_2—Ar—), 14 signals at 123–131 ppm for 15 aromatic C-atoms, two signals being superimposed as demonstrated by the HMBC experiment, see Fig. 14a and three signals at 152–159 ppm (phenolic **C**—O—Ti). Detailed ^{13}C chemical shift values can be found Table 4. One may thus safely conclude that the structure observed in the solid state is conserved in solution and that the complex is rigid enough to keep the quite low P-1 symmetry of the crystal. These well-resolved spectra (21 ^{1}H and 26 ^{13}C signals) also call for an attribution linking each NMR signal to its corresponding crystallographic site in the structure. Thus, a set of 2D NMR experiments was performed in order to identify on ^{1}H and ^{13}C spectra three groups of labels corresponding to the three ligand forms: bhmpc, Hbhmpc and H_2bhmpc.

On the COSY spectrum (Fig. 12), correlation peaks among the methylene signals (**H**—C—**H** correlation part, not shown) confirm and complete the pairing started, relying on J values on the 1D spectrum:

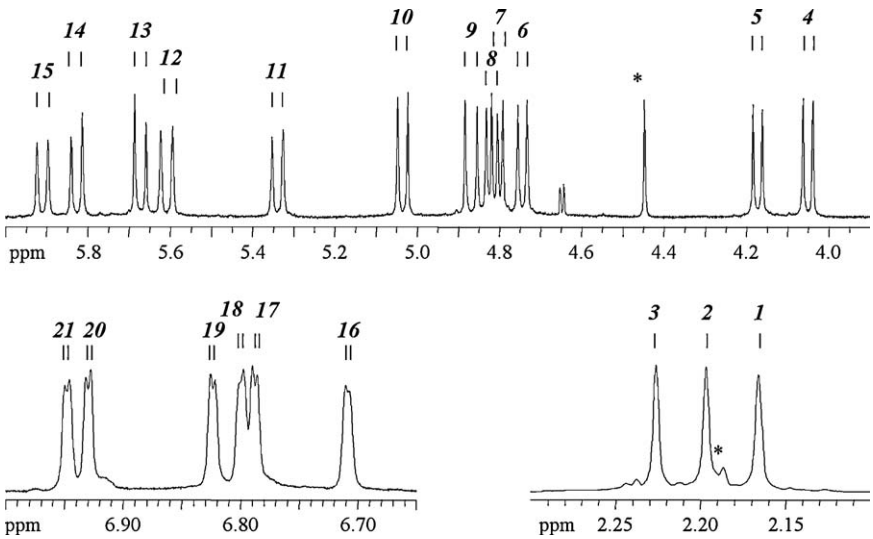

Fig. 10. ^{1}H NMR spectrum of (**1**) dissolved in $CDCl_3$ (0.5 mg/0.6 mL). Signals due to the complex have been arbitrarily labeled from low to high chemical shift values. Signals from residual free ligand H_3bhmpc are marked with an asterisk (see text).

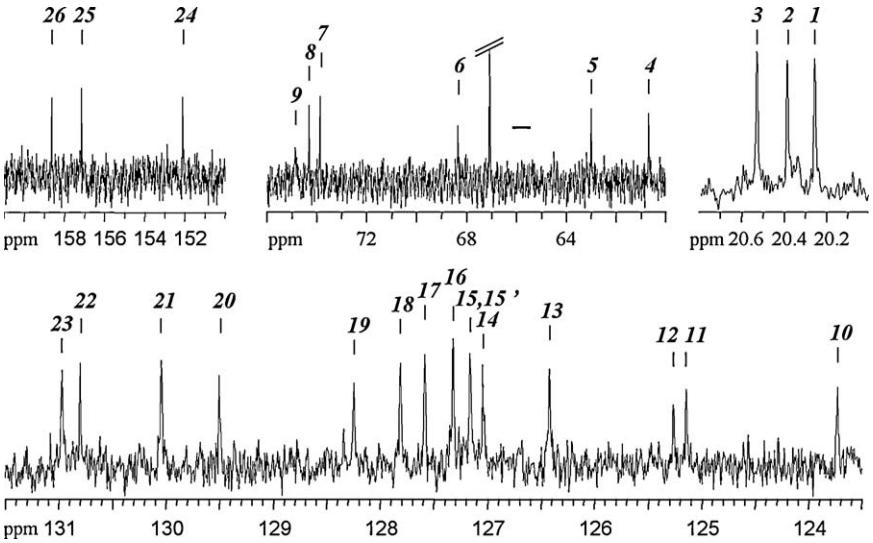

Fig. 11. ^{13}C {1H} NMR spectrum of (**1**) dissolved in $CDCl_3$ (0.5 mg/0.6 mL). Signals due to the complex have been arbitrarily labeled from low to high chemical shift values.

(*H4,H10*), (*H5,H6*), (*H9,H12*), (*H13,H14*), (*H11,H8*) and (*H15,H7*). This information is also available on the **C H**$_2$ correlation part of the HSQC spectrum, Fig. 13a, where ^1H and ^{13}C signals of directly bonded C and H atoms of the six non equivalent CH_2 groups are identified: (*C4,H4,H10*), (*C5,H5,H6*), (*C6,H8,H11*), (*C7,H9,H12*), (*C8,H13,H14*) and (*C9,H7,H15*).

The C**H**—C**H**$_3$ correlation part of the COSY spectrum given in Fig. 12a evidences three subsets of ^1H signals corresponding to aromatic CH and CH_3 groups on each of the three ligand types: (*H1,H16,H18*), (*H2,H19,H20*) and (*H3,H17,H21*). Then HSQC **C**—**H** and **C H**$_3$ correlation parts Fig. 13b and c respectively lead to group CH_3 and CH ^{13}C and ^1H signals the following way *:* (*C1,H1; C13,H16; C17,H18*), (*C2,H3; C21,H17; C18,H21*), (*C3,H2; C16,H19; C23,H20*).

The C**H**$_2$—C**H** correlation part of the COSY spectrum (not shown) does not help to identify CH and CH_2 neighbors readily because of long range couplings ^6J between distant CH and CH_2 in addition to ^4J couplings between close CH and CH_2 on the same ligand. Running a ROESY experiment allows one to investigate ^1H—^1H dipolar interactions and correlates the following pairs of signals: (*H4,H20*), (*H5,H17*), (*H7,H18*), (*H8,H17*), (*H9,H16*), (*H13,H21*), see Fig. 12b. This leads to assign NMR signal labels to CH_3, CH_2 and CH neighbors on the three different ligands. Furthermore each H site of one given CH_2 group can be labeled according to its distance to the neighboring CH given by XRD, see Figs. 8 and 9, making the assumption that the molecular structure is rigid enough, due to intra-molecular H-bonds, to compare that way atoms proximity in solution and in the solid state.

We are then left with the assignment of C-atoms bearing no protons, for which the HMBC spectrum, showing long-range C—H J couplings, has been recorded, see Fig. 14. Among C**H**$_3$—**C** and C**H**$_3$—C—**C**H correlation peaks, Fig. 14c, (*H1,C22*), (*H2,C23*), (*H3,C21*) peaks identify the signals corresponding to the C atoms of each CH_3—**C** fragment. The C**H**—C—**C** O—Ti correlation peaks, Fig. 14b, allows one to label phenolic **C**—O—Ti sites, showing (*H16,H18,C24*), (*H17,H21,C25*), (*H19,H20,C26*) vicinities. Finally, from the C**H**$_2$—**C** and C**H**$_2$—C—**C**H correlation part, Fig. 14a, we get (*H6,C10*), (*H8,H11,C11*), (*H9,H12,C12*), (*H13,H14,C14*), (*H4,H7,H10,H15,C15,C15'*) associations, where the last one can be expressed as (*H7,H15,C15*), (*H4,H10,C15'*), according to the known assignment for the CH_2 protons.

We have thus defined three unambiguous sets of labels for three different ligands:

[C1,H1; C22; (C13,H16; C12; C7,H9,H12); (C17,H18; C15; C9,H7,H15); C24]

[C2,H3; C19; (C21,H17; C10; C5,H5,H6); (C18,H21; C14; C8,H13,H14); C25]

[C3,H2; C20; (C16,H19; C11; C6,H8,H11); (C23,H20; C15'; C4,H4,H10); C26].

At this point, no conclusion has been drawn about the assignment of each of these sets to one specific type of ligand, three protonation states being possible: bhmpc,

Table 4
Partial charges distribution calculated from crystal data, experimental chemical shifts and NMR assignment to crystal sites for heavy atoms contained in (**1**). See Fig. 8 for XRD data labeling, Figs. 9–11 for NMR signals labeling.

Chemical type	XRD label (neighbors)	Charge q	Shift/ppm	NMR label
O atoms	**O1**(Ti1,Ti2,Ti2)	−0.8711	-	-
	O5(Ti1,Ti2,C10)	−0.6666	-	-
	O10(Ti2,C25,Ti1)	−0.6296	-	-
	O2(Ti1,C1)	−0.5400	-	-
	O8(Ti1,C19)	−0.5398	-	-
	O3(Ti1,C7,H41)	−0.5164	-	-
	O9(Ti2,C27)	−0.5084	-	-
	O7(Ti2,C16)	−0.5039	-	-
	O6(C18,H43)	−0.3536	-	-
	O4(C9,H42)	−0.3439	-	-
$CH_3CH_2\underline{O}H$	**O13**(C32,H44)	−0.3420	-	
$\underline{C}H_3CH_2OH$	**C33**(C32,H38,H39,H40)	−0.1181	18.33	
$CH_3\underline{C}H_2OH$	**C32**(O13,C33,H36,H37)	−0.0112	58.37	
Dioxane $\underline{C}_4H_8\underline{O}_2$	**O12**(C29,C30)	−0.2804	-	
	O11(C28,C31)	−0.2757	-	
	C31(O11,C30,H32,H33)	−0.0098	67.06	
	C30(O12,C31,H34,H35)	−0.0072	67.06	
	C29(C28,O12,H28,H29)	−0.0062	67.06	
	C28(O11,C29,H30,H31)	−0.0023	67.06	
Methyle $\underline{C}H_3$	**C26**(C22,H25,H26,H27)	−0.1245	20.26	*C1*
	C8(C4,H19,H20,H21)	−0.1239	20.39	*C2*
	C17(C13,H22,H23,H24)	−0.1237	20.53	*C3*
Aromatic $\underline{C}$—H	**C12**(C11,C13,H3)	−0.0525	127.32	*C16*
	C5(C4,C6,H2)	−0.0524	130.04	*C21*
	C14(C13,C15,H4)	−0.0512	130.97	*C23*
	C21(C20,C22,H5)	−0.0504	126.42	*C13*
	C3(C2,C4,H1)	−0.0474	127.81	*C18*
	C23(C24,H6,C22)	−0.0458	127.58	*C17*
Methylene $\underline{C}H_2$	**C10**(O5,C11,H13,H14)	−0.0539	68.34	*C6*
	C7(C2,O3,H7,H8)	−0.0448	74.32	*C8*
	C27(C24,O9,H15,H16)	−0.0366	74.88	*C9*
	C19(O8,C20,H17,H18)	−0.0307	73.87	*C7*
	C9(C6,O4,H9,H10)	−0.0134	62.98	*C5*
	C18(C15,O6,H11,H12)	−0.0118	60.68	*C4*
Aromatic $\underline{C}$—CH_2O(Ti,H)	**C20**(C19,C21,C25)	−0.0379	125.26	*C12*
	C11(C10,C12,C16)	−0.0330	125.14	*C11*
	C2(C1,C3,C7)	−0.0312	127.04	*C14*
	C24(C23,C25,C27)	−0.0251	127.16	*C15*
	C6(C1,C5,C9)	−0.0130	123.73	*C10*
	C15(C14,C16,C18)	−0.0123	127.16	*C15'*
Aromatic $\underline{C}$—CH_3	**C4**(C3,C5,C8)	−0.0149	128.25	*C19*
	C13(C12,C14,C17)	−0.0142	129.50	*C20*
	C22(C21,C26,C23)	−0.0100	130.80	*C22*
Phenolic $\underline{C}$—O—Ti	**C25**(C24,O10,C20)	+0.0193	152.09	*C24*
	C1(O2,C2,C6)	+0.0407	157.13	*C25*
	C16(C11,C15,O7)	+0.0461	158.63	*C26*
Ti atoms	**Ti2**(O1,O5,O7,O9,O10,O1)	+2.1752	-	-
	Ti1(O1,O2,O3,O5,O8,O10)	+2.4864	-	-

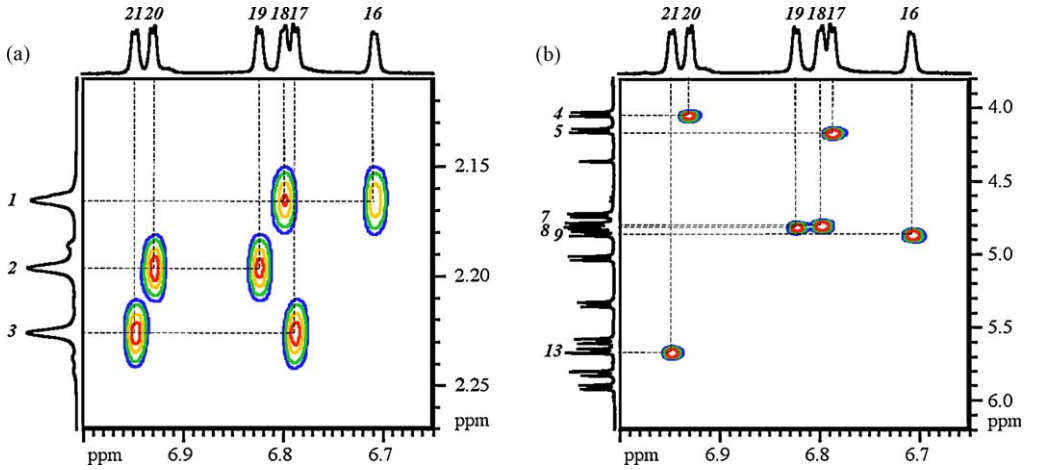

Fig. 12. (a) C**H**—C**H**$_3$ correlation part of the COSY spectrum of (**1**) dissolved in $CDCl_3$, (b) C**H**—C**H**$_2$ correlation part of the ROESY spectrum of (**1**) dissolved in $CDCl_3$.

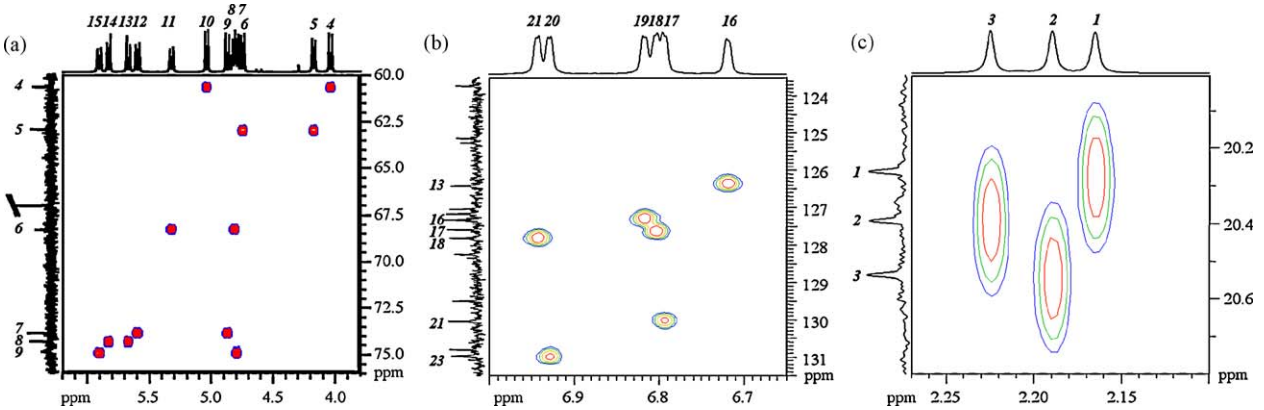

Fig. 13. HSQC spectrum of (**1**) dissolved in $CDCl_3$, (a) **C** **H**$_2$ correlation part, (b) **C**—**H** correlation part, (c) **C** **H**$_3$ correlation part.

Hbhmpc and H_2bhmpc. For that, we can first propose an assignment based on chemical shift arguments and start by considering the six ^{13}C signals corresponding to the methylene moieties (labeled *C4* to *C9* on Fig. 9). From the chemical shift of these moieties in the free ligand H_3bhmpc dissolved in $CDCl_3$ (1 mg / 0.6 mL, spectrum not shown), $\delta = 63.65$ ppm, we propose to assign the two low frequency peaks ($\delta_{C4} = 60.68$ ppm and $\delta_{C5} = 63.00$ ppm) to arms that are not coordinated to Ti-atoms. Then it follows that the two sets containing *C4* and *C5* should correspond to either Hbhmpc or H_2bhpmc, leaving the last set containing *C7* and *C9* for bhmpc. Yet another assignment for the bhmpc ligand is possible by looking at the three ^{13}C signals in the phenolic region (labeled *C24*, *C25* and *C26* on Fig. 9) where one signal (*C24*) appears to be clearly separated from the two other (*C26* and *C27*). Referring to the molecular structure of the complex, it appears that the phenolic O-atoms are in the chelating position for Hbhmpc and H_2bhmpc ligands and in the bridging position for bhmpc. This strongly suggests to assign *C24* to bhmpc, leading to assign the same set of signals as before to this ligand *: [C1,H1; C22; (C13,H16; C12; C7,H9,H12); (C17,H18; C15; C9,H7,H15); C24].* Assuming this attribution is correct, an oriented assignment has to be proposed for this bhmpc ligand. One can notice that one of its O—CH_2 arm is engaged into an intramolecular hydrogen bond with a HO—CH_2 arm of a H_2bhmpc ligand (Fig. 8). If we look for the available protons around this H-bonded arm in the molecular structure, we found at a distance less than 320 pm one O—H bond and three C—H bonds. The situation is completely different for the other arm where it comes six C—H bonds (four from CH groups and two from CH_2 groups). Noticing the broadness of the *C9* signal compared to the *C7* one particularly, it is

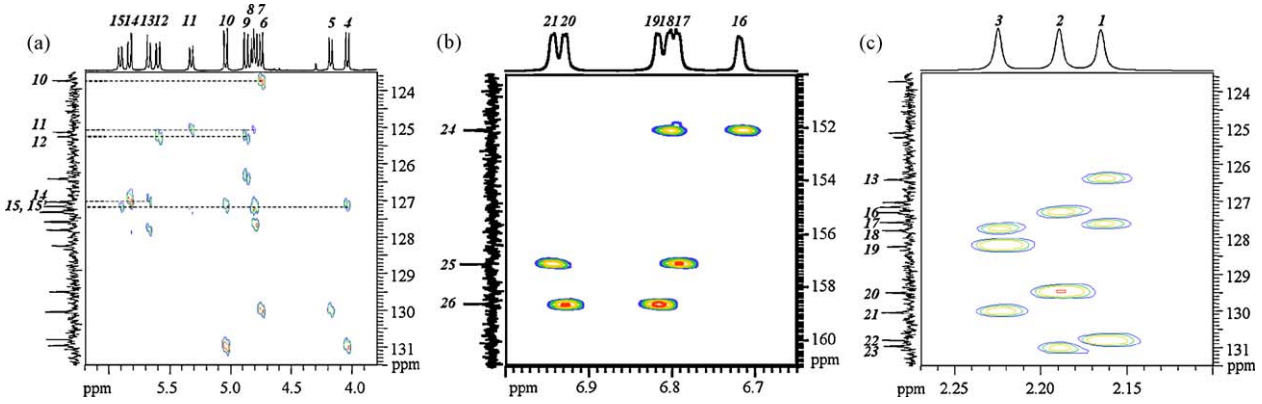

Fig. 14. HMBC spectrum of (**1**) dissolved in $CDCl_3$, (a) C**H**$_2$—**C** and C**H**$_2$—C—**C**H correlation part, (b) C**H**—C—**C**—O—Ti correlation part, (c) C**H**$_3$—**C** and C**H**$_3$—C—**C**H correlation part.

tempting to assign *C9* to the H-bonded arm, for which H-bond might well lead to chemical shift distribution and/or shorter transversal relaxation time T_2, and *C7* to the non H-bonded one. A complete assignment is then proposed for the bhmpc ligand.

The two remaining sets are still to be assigned either to Hbhmpc or H_2bhmpc. The Ti-bonded O**C**H$_2$ zone in the ^{13}C NMR spectrum shows three rather close peaks (*C7,C8, C9*), separated from a single peak (*C6*). In the molecular structure, two situations also appear: three similar Ti—O**C**H$_2$—Ar arms (two in bhmpc, one in H_2bhmpc) and the (Ti)$_2$—O**C**H$_2$—Ar arm belonging to the Hbhmpc form. Then, *C6* can be assigned to the Hbhmpc form, leaving *C8* for the H_2bhmpc one, as *C7* and *C9* are already supposed to belong to bhmpc. Considering the identified sets of signals, it follows that *C4* belongs to the free arm of Hbhmpc and *C5* to the free arm of H_2bhmpc. Then we have reached a complete assignment of the ^{13}C NMR spectra, inducing a complete assignment of the ^{1}H NMR spectra as well.

In order to validate these assignments, we have also measured the longitudinal relaxation times T_1 of both ^{1}H and ^{13}C nuclei in our complex. For the ^{13}C nuclei, we found that relaxation times were ruled by the first coordination sphere as all values for a given type of chemical group are very similar (standard deviation is given in brackets): T_1(—**C**H$_2$) = 0.135(14) s, T_1(—**C**C$_2$H) = 0.22(3) s, T_1(—**C**H$_3$) = 0.81(7) s, T_1(—**C**C$_3$) = 0.83(13) s and T_1(—**C**C$_2$O) = 1.24(17) s, with no significant differences observed among the three protonation states. The situation was very similar concerning ^{1}H relaxation times of methyl T_1(—C**H**$_3$) = 0.822(6) s or aromatic CH groups T_1(—C**H**) = 1.34(6) s, but not with methylene groups where significant differences were observed T_1(—C**H**$_2$) = 0.401(34) s, see Table 5. Two protons belonging to the same methylene group are expected to reveal similar T_1 values if mobility allows them to explore a same mean environment. On the contrary, if their mobility is restrained, different sensed environments will lead to significantly different relaxation times. When comparing the two relaxation times measured for each proton belonging to the same methylene group (identified below by its C atom NMR label), three cases may be encountered:

- almost no differentiation: $\Delta T_1(C5) = 1$ ms and $\Delta T_1(C7) = 8$ ms;
- moderate differentiation: $\Delta T_1(C4) = 37$ ms and $\Delta T_1(C8) = 57$ ms;
- strong differentiation: $\Delta T_1(C9) = 94$ ms and $\Delta T_1(C6) = 112$ ms.

A large ΔT_1 being associated to a high rigidity of the CH_2 arm, we can assign the largest ΔT_1 (protons on *C6*) to the most constrained μ_2-CH_2OTi_2 bridge occurring in the Hbhmpc ligand. This single observation is enough to validate in an independent way the previously derived assignment. It also explains the satisfactory correlation shown in Fig. 15 concerning the relationship between observed ^{1}H T_1-values and $(\Sigma\ 1/r^6)^{-1}$ values computed according to the proposed NMR assignment using the available structural data (H-atoms neighbors at less than $r = 300$ pm distance).

3.7. Assignment directly from crystal structures

The above results show how it was possible to establish on a purely experimental basis a link between the solid-state molecular structure of a sol–gel precursor

Table 5
^{13}C {^{1}H} and ^{1}H T_1-values measured for CH_2 fragments, displayed according to our assignment of signals to the three different ligands. Standard deviation is given in brackets.

Ligand	NMR label	^{13}C T_1 (ms)	NMR label	^{1}H T_1 (ms)
bhmpc	*C7*	148(27)	*H9*	406(3)
			H12	414(3)
	C9	126(31)	*H7*	353(4)
			H15	447(3)
Hbhmpc	*C4*	156(18)	*H4*	421(3)
			H10	384(2)
	C6	116(30)	*H8*	332(5)
			H11	444(5)
H_2bhmpc	*C5*	125(10)	*H5*	396(24)
			H6	397(2)
	C8	140(13)	*H13*	381(8)
			H14	438(4)

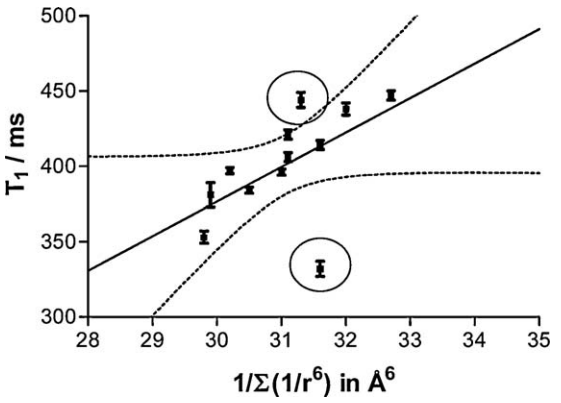

Fig. 15. Correlation between ^{1}H nuclei longitudinal relaxation times of methylene groups and the inverse of the sum over H-neighbors located at less than 300 pm from the concerned nucleus of the inverse of sixth power of H. . .H distance. NMR Assignment of Fig. 9 and distances extracted from XRD data (Fig. 8) has been used to produce this plot. See discussion for the two points falling outside the 95% confidence hyperbolae (dotted lines).

and its associated high-resolution ^{1}H and ^{13}C NMR solution spectra. The problem is that such a full assignment is quite expensive in terms of NMR-recording time and the question is now asked if such an assignment could be made directly from available crystalline data. The principal motivation for such a theoretical analysis is the high-quality partial charges derived from the PACHA algorithm [34] and the fact that two crystal structures are available for the same structural motif differing only by the kind of solvent molecules filling the holes in the lattice [33]. Through the aid of Eq. (1), it becomes then possible to quantify in terms of chemical shifts the effect of replacing ethanol by chloroform, thereby allowing diving more deeply into the origin of these ^{13}C chemical shifts.

As explained in the theoretical section, the first job is to fix reasonable values for the two critical parameters of the model, the f-factor ruling the charge dependence of the inverse electron–nucleus cubed distance r averaged over 2p-orbitals $< (a_0/r)^3 >_{2p} = R^{\circ} \cdot (1 - f \cdot q)$ and average excitation energy ΔE. As the partial charges given by the PACHA software are of *ab initio* quality [34], we have set $f = 1$ as suggested by computations based on Hartree–Fock–Slater-type orbitals [48,66]. The only adjustable parameter in the modeling was thus the average excitation energy, whose value is generally ruled by the nature of the first coordination sphere of the ^{13}C nucleus. In the present case, the experimentally observed ^{13}C resonances have been grouped into five (free ligand) and six (tetranuclear complex) different sets differing by the nature and number of atoms within the first coordination sphere of the carbon-atom (Table 6). For each set, an average chemical shift was computed, leading after inversion of equation (1) to an associated ΔE-value also indicated in Table 6. Furthermore, a comparison between the ΔE-values deduced from the structure of the free ligand (H_3bhmpc, MUGNAD code in the Cambridge Structural Database) and that of the two complexes shows, as expected, a pretty good constancy for all C-sites not linked to oxygen atoms. For the two carbon sites linked to O—Ti moieties, a significant ΔE-decrease is observed relative to the ligand, responsible for the observed deshielding of the associated resonances in the NMR spectrum. Another point of interest of this table lies in the easy identification of the phenolic ''C—C—O'' groups as the least affected set of resonances by the substitution EtOH → CHCl3, owing to the perfect invariance of the corresponding ΔE-values. With Table 6, it is now possible by direct application of Eq. (1) to transform the partial charges given by the PACHA algorithm into ^{13}C NMR chemical shifts.

Table 7 shows the NMR shifts predicted for the ethanol solvate structure while Table 8 refers to the chloroform solvate structure. Owing to the quite low polarities of these highly covalent bonds ($-0.18 < q_C < +0.05$), the population unbalance contribution P_u is clearly not the dominant factor for explaining the observed chemical shift variations. For the same reason, the diamagnetic contribution σ_{dia}, remains stuck around 284 ppm (absolute shielding scale). It may thus be concluded, in agreement with more sophisticated approaches, that the dominant contribution to the ^{13}C chemical shifts is due to the variation of the paramagnetic term either through the

Table 6
Average ^{13}C NMR chemical shifts and associated average excitation energy ΔE computed for each kind of first coordination sphere observed for carbon atoms in H_3bhmpc and (**1**) allowing prediction of ^{13}C NMR chemical shifts directly from the crystalline structure.

	Average shift /ppm	ΔE/eV
Free ligand		
C—C—O	149.88	7.67
C—C—H	126.79	7.51
C—C—C	128.11	7.77
C—(OH)—H—H	59.78	11.09
Ph—H—H—H	20.85	13.19
Complex		
C—C—(OTi)	155.95	7.25 (7.25)
C—C—H	128.36	7.49 (7.37)
C—C—C	127.10	7.68 (7.78)
C—(OTi)—H—H	72.85	9.95 (9.69)
C—(OH)—H—H	61.83	10.95 (10.63)
Ph—H—H—H	20.39	13.08 (12.32)

average excitation energy for C-sites differing in their first coordination sphere or through the inverse electron–nucleus cubed distance r averaged over 2p-orbitals $< (a_0/r)^3 >_{2p}$ for C-sites sharing the same first coordination sphere. The high quality of our charge modeling is again well reflected by looking at the predicted values for $C_2\underline{\mathbf{C}}$—O sites deduced from the crystal data concerning ethanol and chloroform solvates. In both cases, the observed experimental ordering δ(H-bhmpc) > δ(H_2bhpmc) >> δ(bhmpc) is quantitatively reproduced with less than 0.3 ppm and 0.7 ppm errors for the ethanol and chloroform cases, respectively. This right assignment based on two different crystal data rules completely out the possibility of a by-chance result. Obviously, such an agreement with solution NMR data for these $C_2\underline{\mathbf{C}}$—O sites comes from the fact that they are deeply buried in the most rigid part of the complex and are thus not under the influence of moving solvent molecules. Consequently, the next step is to look at aromatic $C_2\underline{\mathbf{C}}$—C sites that are also expected to be least affected by the presence of solvent molecules. The observed experimental ordering δ(bhmpc) > δ(Hbhpmc) > δ(H_2bhmpc) for the three $H_3\underline{\mathbf{C}}$—Ph sites (C22, C20 and C19 resonances) is here also quantitatively reproduced with errors less than 0.5 ppm for C20 (Hbhmpc) and C22 resonance (bhmpc) in the ethanol and chloroform cases, respectively. Interestingly enough, the least rigid H_2bhmpc ligand (C19 resonance) is characterized by a larger error

Table 7
Prediction of ^{13}C NMR chemical shifts from the ethanol solvate structure using Table 6.

Site	Type	Charge q	σ_{dia}/ppm	$<(a_0/r)^3>$ /au	Pu	δ_{calc}/ppm	δ_{exp}/ppm
C26	CCO	+0.04610	283.84	1.28670	1.49965	158.67	158.63
C25	CCO	+0.04067	283.89	1.28002	1.49972	157.30	157.13
C24	CCO	+0.01926	284.09	1.25369	1.49994	151.88	152.09
C23	CCH	−0.05120	284.21	1.16703	1.49956	126.80	130.97
C21	CCH	−0.05240	284.20	1.16555	1.49954	126.51	130.04
C18	CCH	−0.04740	284.21	1.17170	1.49963	127.71	127.81
C17	CCH	−0.04580	284.21	1.17367	1.49965	128.09	127.58
C16	CCH	−0.05252	284.20	1.16541	1.49954	126.49	127.32
C13	CCH	−0.05042	284.21	1.16798	1.49958	126.99	126.42
C22	CCC	−0.00996	284.25	1.21775	1.49998	130.99	130.80
C20	CCC	−0.01419	284.24	1.21255	1.49997	130.01	129.50
C19	CCC	−0.01493	284.24	1.21164	1.49996	129.84	128.25
C15	CCC	−0.02509	284.23	1.19913	1.49990	127.48	127.16
C15’	CCC	−0.01232	284.25	1.21485	1.49997	130.44	127.16
C14	CCC	−0.03119	284.23	1.19164	1.49984	126.06	127.04
C12	CCC	−0.03794	284.22	1.18333	1.49976	124.49	125.26
C11	CCC	−0.03296	284.22	1.18946	1.49982	125.65	125.14
C10	CCC	−0.01301	284.24	1.21400	1.49997	130.28	123.73
C9	COHH	−0.03661	284.22	1.18497	1.49978	73.73	74.88
C8	COHH	−0.04479	284.21	1.17491	1.49967	72.26	74.32
C7	COHH	−0.03072	284.23	1.19221	1.49984	74.79	73.87
C6	COHH	−0.05387	284.20	1.16374	1.49952	70.63	68.34
C5	COHH	−0.01339	284.24	1.21353	1.49997	61.70	62.98
C4	COHH	−0.01182	284.25	1.21546	1.49998	61.96	60.68
C3	CHHH	−0.12369	284.13	1.07786	1.49745	20.44	20.53
C2	CHHH	−0.12392	284.13	1.07757	1.49744	20.41	20.39
C1	CHHH	−0.12449	284.13	1.07688	1.49742	20.33	20.26

Table 8
Prediction of ^{13}C NMR chemical shifts from the chloroform solvate structure using Table 6.

Site	Type	Charge q	σ_{dia}/ppm	$<(a_0/r)^3>$/au	Pu	δ_{calc}/ppm	δ_{exp}/ppm
C26	CCO	+0.04308	283.96	1.28298	1.49969	157.94	158.63
C25	CCO	+0.04153	283.89	1.28109	1.49971	157.55	157.13
C24	CCO	+0.02103	284.07	1.25587	1.49993	152.36	152.09
C23	CCH	−0.06504	284.19	1.15001	1.49930	127.12	130.97
C21	CCH	−0.06305	284.19	1.15245	1.49934	127.61	130.04
C18	CCH	−0.05434	284.20	1.15856	1.49944	128.82	127.81
C17	CCH	−0.05268	284.20	1.16316	1.49951	129.73	127.58
C16	CCH	−0.06243	284.19	1.15321	1.49935	127.76	127.32
C13	CCH	−0.05677	284.20	1.16018	1.49947	129.14	126.42
C22	CCC	0.00309	284.23	1.23380	1.50000	130.87	130.80
C20	CCC	−0.00249	284.26	1.22694	1.50000	129.43	129.57
C19	CCC	−0.00431	284.25	1.22471	1.50000	129.16	128.25
C15	CCC	−0.01635	284.25	1.20990	1.49995	126.40	127.16
C15’	CCC	−0.01111	284.25	1.21634	1.49998	127.60	127.16
C14	CCC	−0.02615	284.23	1.19784	1.49994	124.16	127.04
C12	CCC	−0.02544	284.23	1.19872	1.49994	124.32	125.26
C11	CCC	−0.02790	284.23	1.19569	1.49987	123.76	125.14
C10	CCC	−0.00901	284.25	1.21892	1.49999	128.08	123.73
C9	COHH	−0.06249	284.19	1.15314	1.49935	73.56	74.88
C8	COHH	−0.07103	284.19	1.14264	1.49916	71.98	74.32
C7	COHH	−0.06151	284.20	1.15435	1.49937	73.74	73.87
C6	COHH	−0.07019	284.19	1.14367	1.49918	72.13	68.34
C5	COHH	−0.03686	284.22	1.18467	1.49977	62.63	62.98
C4	COHH	−0.04632	284.21	1.17303	1.49964	61.04	60.68
C3	CHHH	−0.17742	284.07	1.01178	1.49476	19.93	20.53
C2	CHHH	−0.17380	284.07	1.01623	1.49497	20.46	20.39
C1	CHHH	−0.17153	284.08	1.01902	1.49510	20.80	20.26

(1.6 ppm) in EtOH than in $CDCl_3$ (1.0 ppm). This slightly larger error does not affect the predicted assignment, nor the fact that the $H_3\underline{C}$—Ph resonances should all be deshielded relative to Ph$\underline{C}$—CH_2O resonances. For these last signals, the agreement between calculated and experimental positions is found to be acceptable (errors less than 1.5 ppm) for C11, C12, C14, C15 resonances (Table 7) in the case of the ethanol solvate and for C12, C15, C15’ resonances (Table 8) in the case of the chloroform solvate. Most interesting is the large 3 ppm error in the position of the C15’ resonance, experimentally assigned to the Ph$\underline{C}$—CH_2—(OH)...H arm of a Hbhmpc ligand, in the ethanol solvate case that is reduced down to 0.4 ppm in the chloroform solvate case. It may then be deduced that the H-bonded structure in which the ethanol molecule is engaged in the ethanol solvate is most probably broken after dissolution of the crystals in $CDCl_3$. It is worth noticing that for the other coordinated Ph$\underline{C}$—CH_2—(OTi_2) arm of this Hbhmpc ligand (C11 resonance), the error is lower in the ethanol solvate case (0.5 ppm) relative to the chloroform case (1.4 ppm). This would suggest that we have not a complete ethanol-chloroform substitution upon dissolution, but just a significant rearrangement of the H-bond pattern in order to accommodate both ethanol and chloroform around the structure. As expected, the prediction for the C15 and C12 resonances assigned respectively to Ph$\underline{C}$—CH_2—(OTi)...H and Ph$\underline{C}$—CH_2—(OTi) arms of a bhmpc ligand are quite good in both cases (errors less than 1 ppm) while that concerning the C10 and C14 resonances assigned to the two arms of H_2bhmpc ligands are the worst ones with errors larger than 1 ppm. For the C10 resonance associated to the uncoordinated Ph$\underline{C}$—CH_2—(OH)...H arm, a large error is systematically observed. It is, however, logically smaller for the $CDCl_3$ case (4.4 ppm) relative to the EtOH case (6.6 ppm). As already observed in the Hbhmpc case, errors are reversed concerning the other coordinated Ph$\underline{C}$—CH_2—(OH)—Ti arm (C14 resonance) with a better agreement (about 1 ppm error) for the ethanol solvate compared to the chloroform solvate (about 3 ppm error). Here also, a rearrangement of the H-bond pattern around the H_2bhmpc ligands specific to the solution is probably responsible for the difficulty to reproduce the observed chemical shifts using crystalline data alone.

Up to now, focus has been put on C-atoms bearing no protons because these atomic sites were expected to be the least affected by dissolving the crystals in $CDCl_3$, whereas protonated sites such as methine, methylene and methyl groups are expected to be in direct van der Waals contact with solvent molecules. For these groups, there is thus no a priori reason to expect a correlation between NMR data recorded in solution and structural data derived from single-crystal X-ray diffraction. Nevertheless, if such correlations are observed for some selected sites of the molecule, it could be concluded that the solvent is very probably excluded from the considered region. Obvious reasons for such an exclusion could be either an unfavourable steric interaction or even an entropic factor linked to the existence of very particular H-bonding scheme involving several kinds of small molecules. This is precisely the case here, with ethanol, dioxane and chloroform competing for the solvatation of the same double-calix shaped complex. The aromatic methine groups being the most buried sites, it is thus not surprising to find that using the ethanol solvate structure (Table 7), the relative positions of four resonances (C13, C16, C17, C18) among six possibilities are correctly predicted with less than 1 ppm error. Interestingly enough, these four sites are precisely those having in ortho position a Ti-coordinated arm: C13(bhmpc) = H**C**—Ph—CH_2—OTi, C16(Hbhmpc) = H**C**—Ph—CH_2—OTi_2, C17(bhmpc) = H**C**—Ph—CH_2—(OTi)...H and C18(H_2bhmpc) = H**C**—Ph—CH_2—(OH)Ti. Comparison with the chloroform solvate case (Table 8) then shows that the position of only two resonances (C16 and C18) are predicted with less than 1 ppm error. In this case, the two methine resonances associated to the bhmpc ligand (C13 and C17) are strongly affected (error of 2.7 and 2.3 ppm respectively). It may thus be concluded that, in solution, chloroform molecules are most probably excluded from the neighborhood of the bhmpc ligand, interacting more selectively with the less rigid Hbhmpc and H_2bhmpc regions. Large errors (more than 2 ppm) are observed in both solvates for the two other sites, C21(H_2bhmpc) and C23(Hbhmpc), having in ortho position an uncoordinated H**C**—Ph—CH_2—(OH)...H arm, evidencing as before a specific reorganisation of the intramolecular H-bond pattern in solution. In strong contrast with methine groups, errors larger than 1 ppm are systematically observed (Table 7) for the six resonances of the methylene groups using ethanol solvate crystal data. On the other hand, three very good predictions with errors less than 0.5 ppm can be observed: C7(bhmpc) = Ph**C**H_2—(OTi), C5(H_2bhmpc) = Ph**C**H_2—(OH)...O and C4(Hbhmpc) = Ph**C**H_2—(OH)...O, for the chloroform solvate case (Table 8). This observation strongly suggests that chloroform molecules should have a good affinity for such sites and is in perfect coherence with the errors larger than 1 ppm observed for the three other methylene sites that are much more crowded and thus less accessible to $CDCl_3$: C9(bhmpc) = Ph**C**H_2—(OTi)...H, C8(H_2bhmpc) = Ph**C**H_2—(OH)Ti...O and C6(Hbhmpc) = Ph**C**H_2—(OTi_2). At last, it was possible to predict with an error less than 0.5 ppm, the relative positions of the three resonances arising from the H_3**C**—Ph sites, using the ethanol solvate crystal data. Corresponding errors being one order of magnitude larger using the chloroform solvate data, it may be safely concluded that ethanol molecules are most probably selectively located in the neighbourhood of these methyl groups, thus preventing the approach of the solvent molecules.

4. Discussion

Sol–gel precursors containing Ti(IV) centers are usually colorless and highly reactive compounds towards moisture showing a variable degree of association dependent on the solvent used. This is not the case of the orange-red compound studied here that displays a quite rigid tetrameric brucite-type core (named ''brucitane'' hereafter) that is perfectly stable under ambient atmosphere. Being self-assembled in large yields at room temperature from any kind of commercial $Ti(OR)_4$ alkoxide after reaction with H_3bhmpc using 1,4-dioxane as a solvent, we think that (**1**) should be a perfect molecular precursor for building hybrid oganic–inorganic nanoporous TiO_2-based materials displaying a significant absorption I the visible part of the electromagnetic spectrum. This is the reason why a complete spectroscopic characterization of this important precursor has been presented that should be very useful for future sol–gel synthesis involving it. ^{13}C CPMAS NMR measurements have shown that upon drying ethanol molecules can be removed from the crystals without destroying the molecular structure of the complex. This demonstrates the good stability of this complex under ambient atmosphere, conditions under which most Ti(IV) precursors are irreversibly hydrolyzed to white powders. NMR studies has also shown that if the synthetic pathway leads in a highly reproducible way to the same molecular unit, stacking of this unit in the solid state to yield a crystal was a rather subtle process leading to at least four crystalline polymorphs. Last, but not least, 2D NMR techniques has also allowed us to propose a complete assignment of

both solution ^{1}H and ^{13}C spectra that has been used to check the capabilities of the PACHA approach in predicting ^{13}C NMR chemical shifts directly from the molecular structure, a notable difficult problem. The high quality of the partial charges distribution computed for the ethanol and chloroform solvates (Tables 7 and 8) is illustrated by the very reasonable ΔE-values derived from the knowledge of the average chemical shift. Moreover, the order found $\Delta E(sp^2, \pi\rightarrow\pi^*) < \Delta E(sp^3, n\rightarrow\sigma^*) < \Delta E(sp^3, \sigma\rightarrow\sigma^*)$ was well in line with results that would have been deduced from qualitative molecular orbital theory. The ΔE-decrease relative to the free ligand observed for the two carbon sites linked to O—Ti moieties is also well in line with qualitative MO-theory that would place the d-empty d-orbitals of Ti-atoms far above the (n,σ,π)-HOMOs and slightly below the (σ^*,π^*)-LUMOs. One may be tempted to correlate the ΔE-values derived in Table 6 with the U.V.-Vis. absorption bands of the free ligand or the complex (Fig. 2) that corresponds to HOMO-LUMO energies of 5.3, 4.4 and 3.6 eV. The fact that both sets of values are different within a factor of 2 should not be surprising as optical transitions are rule by electric dipole selection rules, whereas chemical shifts are ruled by magnetic dipole selection rules.

Yet another way to use our partial charges consists in summing individual atomic charges according to the stoichiometry of meaningful moieties in the structure. For instance, in the case of the ethanol solvate structure the following global charge distribution is obtained:

$$[\{Ti_2O\}^{+3.79}(H_2bhmpc)^{-0.86}(Hbhmpc)^{-1.18}(bhmpc)^{-1.58}.(C_4H_8O_2)^{-0.18}.(EtOH)^{+0.01}]_2$$

This allows discussing on a quantitative basis ionic characters for each moiety by making reference to a perfectly ionic situation derived by considering standard oxidation numbers: $[\{Ti_2O\}^{+6}(H_2bhmpc)^{-1}(Hbhmpc)^{-2}(bhmpc)^{-3}.(C_4H_8O_2)^{0}.(EtOH)^{0}]_2$. Comparison of these two formulas thus nicely explains why ethanol molecules are readily eliminated from the structure under ambient atmosphere owing to their almost zero slightly positive charge. This also explains why 1,4-dioxane molecules are not eliminated from the two cavities under similar conditions owing to a significant overall negative charge easily attracted by the strong positive charge on $\{Ti_2O\}$ moieties. This excess small negative charge on 1,4-dioxane is also probably responsible for the overall weakening of the vibration bands of this molecule observed through IR and Raman spectroscopies. Referring to the fully ionic situation $\{Ti_2O\}^{+6}$, one may say that the ionic character of the titanium oxo core is about 63%. This value should be compared to the ionic character found in TiO_2 polymorphs, using the same PACHA algorithm, that are either 39% (TiO_2—R and TiO_2—H), 41% (rutile, anatase, brookite, TiO_2—B, TiO_2—II) or 44% (TiO_2—III) [1]. This increase in ionicity is quite logical as it merely means that oxide O^{2-} anions are much better electron donors than H_2bhmpc^-, $Hbhmpc^{2-}$ or $bhmpc^{3-}$ anions. Associated ionic characters for these three ligands are found to decrease in the order H_2bhmpc^- (86%) > $Hbhmpc^{2-}$ (59%) > $bhmpc^{3-}$ (53%), reflecting again their different electron donor abilities. It may be worth comparing these ionic characters to those found in crystalline H_3bhmpc (CSD code MUGNAD): H_2bhmpc^- (23%) > $Hbhmpc^{2-}$ (22%) = $bhmpc^{3-}$ (22%). This illustrates the strong electron donor ability of Ti-atoms relative to H-atoms. The same analysis may also be performed for the two non-equivalent tetramers found in the unit-cell of the chloroform solvate:

$$[\{Ti_2O\}^{+3.78}(H_2bhmpc)^{-0.67}(Hbhmpc)^{-1.04}(bhmpc)^{-1.42}.(C_4H_8O_2)^{-0.12}.(CHCl_3)^{-0.28}]_2$$

$$[\{Ti_2O\}^{+3.76}(H_2bhmpc)^{-0.76}(Hbhmpc)^{-1.03}(bhmpc)^{-1.44}.(C_4H_8O_2)^{-0.10}.(CHCl_3)^{-0.32}]_2.(CHCl_3)^{-0.35}$$

This shows that replacing ethanol by chloroform has no effect on the ionic character of the titanium oxo core (63%) but reduces significantly the excess negative charge on 1,4-dioxane molecules as well as the ionic characters of the ligands: H_2bhmpc^- (67–76%) > $Hbhmpc^{2-}$ (52%) > $bhmpc^{3-}$ (47–48%).

Fig. 16 shows the generated geometries and their associated self-energies and standard entropies for the thermodynamic modeling of the complexation of titanium alkoxides by H_3bhmpc ligands in 1,4-dioxane/ROH mixtures. The case of $Ti(OPr^i)_4$ will be considered first as all spectroscopic studies and molecular weight measurements agree with the tetrahedral monomeric nature of this precursor. The only incertitude thus concerns the structure adopted in solution by the H_3bhmpc ligand able to form two stable intramolecular hydrogen bonds. Assuming that dioxane inclusion comes after formation of the complex, we may consider the following stoichiometric equation:

$$4Ti(OPr^i)_4 + 6H_3bhmpc(intra) + 2H_2O \rightarrow 16\,^iPrOH + \{[Ti_2O(bhmpc)(Hbhmpc)(H_2bhmpc)]\}_2$$

Using the thermodynamic data given in Fig. 16, it comes $\Delta H = +1100$ kJ.mol^{-1} and $\Delta S = +1223$ J.mol^{-1}.K^{-1} leading to $\Delta G_{300K} = +733$ kJ.mol^{-1}.

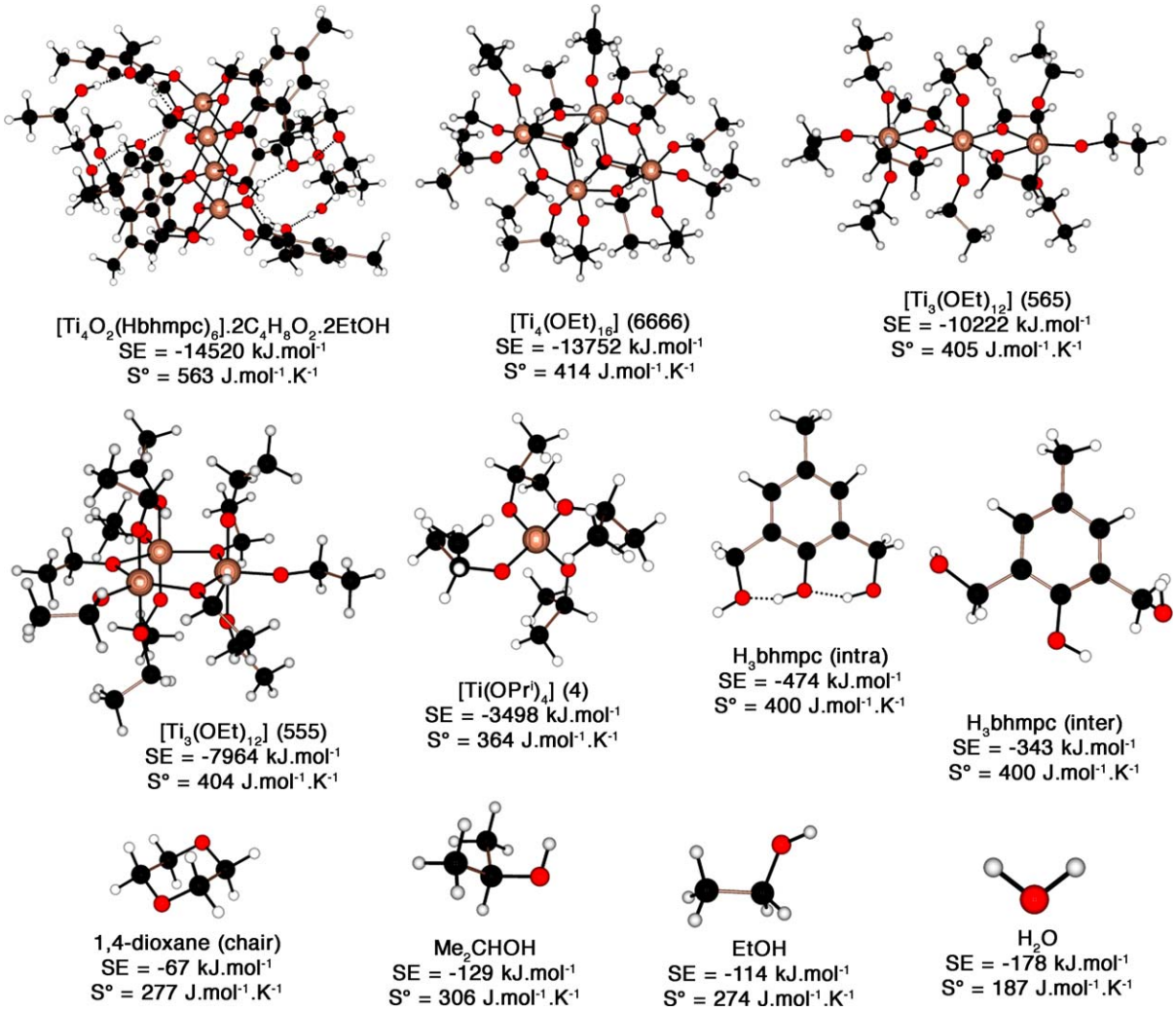

Fig. 16. Self-energies and standard entropies for reactants and products according to the PACHA formalism. Color code: titanium atoms in wood, oxygen atoms in red, carbon atoms in black and hydrogen atoms in grey. Dotted lines refer to hydrogen bonds. The thermodynamic parameters for a complex not solvated by ethanol molecules $\{[Ti_2O(bhmpc)(Hbhmpc)(H_2bhmpc)].C_4H_8O_2\}_2$ are SE = 14232 kJ.mol^{-1} and S° = 561 J.mol^{-1}.K^{-1}. Removal of the two dioxane molecules from the cavities to form $\{[Ti_2O(bhmpc)(Hbhmpc)(H_2bhmpc)]\}_2$ leads to SE = 14028 kJ.mol^{-1} and S° = 557 J.mol^{-1}.K^{-1}.

Considering the simultaneous dioxane inclusion within the two divergent cavities leads to a slightly less endothermic process (ΔH = +1030 kJ.mol^{-1}) but leads also to a large drop in entropy (ΔS = +673 J.mol^{-1}.K^{-1}) owing to the loss of both rotational and solution entropies of these two molecules. The large positive value, ΔG_{300K} = +828 kJ.mol^{-1} entirely due to the highly endothermic enthalpic term shows that reactants are too stabilized to react. In order to destabilize the precursors, one may thus either increase the Ti—O bond length in Ti(OPr^i)$_4$ or break the two intramolecular H-bonds assumed to occur in the H$_3$bhmpc ligand. As the Ti—O bond length has already been elongated (1.84 Å in solution against 1.77 Å in the pure liquid), its seems logical to investigate the effect of H-bonds breaking:

$$4\mathrm{Ti(OPr^i)_4} + 6\mathrm{H_3bhmpc(inter)} + 2\mathrm{H_2O} \rightarrow 16\,\mathrm{^iPrOH} + \{[\mathrm{Ti_2O(bhmpc)(Hbhmpc)(H_2bhmpc)}]\}_2$$

Owing to the destabilization of the ligand that has a negligible effect on the entropy term, the reaction is now significantly less endothermic with ΔH = +314 kJ.mol^{-1} leading to a favorable free energy decrease: $\Delta G_{300K} = -53$ kJ.mol^{-1}. Considering as before the simultaneous dioxane inclusion within the two divergent cavities leads ΔH = +244 kJ.mol^{-1}, i.e. to

$\Delta G_{300K} = +42$ kJ.mol^{-1}. It may thus faithfully be concluded that the complexation of $Ti(OPr^i)_4$ by H_3bhmpc is a completely entropy-driven reaction and that solvents allowing this complexation are those that are able to prevent formation of intramolecular H-bonds between the OH moieties of the H_3bhmpc ligand that is obviously the case for alcohols/dioxane mixtures.

The case of $Ti(OEt)_4$ is more difficult to handle owing to the controversies existing in literature concerning its molecular structure known to be a tetramer in the solid state [58] and a trimer in ultra-dry benzene [67,68]. Considering that (**1**) and $[Ti_4(OEt)_{16}]$ share the same characteristic brucitane $\{Ti_4O_{16}\}$ core in the solid state and that H_3bhmpc reacts under a non-H-bonded structure, let us first assume that the reaction proceeds along the following equation:

$$[Ti_4(OEt)_{16}] + 6H_3bhmpc(intra) + 2H_2O + 2C_4H_8O_2 \rightarrow 14EtOH + \{[Ti_2O(bhmpc)(Hbhmpc)(H_2bhmpc)].C_4H_8O_2.EtOH\}_2$$

From the data given in Fig. 16, we get $\Delta H = +184$ kJ.mol^{-1} and $\Delta S = +657$ J.mol^{-1}.K^{-1} leading to $\Delta G_{300K} = -13.1$ kJ.mol^{-1}. In contrast with the $Ti(OPr^i)_4$ case and despite being an overall endothermic process, there is enough entropy to bind with the complex two dioxane and ethanol molecules in agreement with the solid state structure. Let us then consider the case of a complex not solvated by ethanol molecules:

$$[Ti_4(OEt)_{16}] + 6H_3bhmpc(inter) + 2H_2O + 2C_4H_8O_2 \rightarrow 16EtOH + \{[Ti_2O(bhmpc)(Hbhmpc)(H_2bhmpc)].C_4H_8O_2\}_2$$

From Fig. 16, it comes: $\Delta H = +244$ kJ.mol^{-1} leading with $\Delta S = +1203$ J.mol^{-1}.K^{-1} to $\Delta G_{300K} = -117$ kJ.mol^{-1}. This shows that the enthalpy destabilization coming from the breaking of the two H-bonds is more than compensated by the entropic stabilization gained by the liberation of two ethanol molecules. Considering the effect of further removal of the two dioxane molecules comes $\Delta H = +314$ kJ.mol^{-1} leading, with $\Delta S = +1757$ J.mol^{-1}.K^{-1} to $\Delta G_{300K} = -213$ kJ.mol^{-1}. This shows that encapsulation of dioxane molecules is by itself not a favorable process being significantly endothermic and having a rather high entropic cost. It may nevertheless readily occur at room temperature owing to its coupling with the liberation in solution of all the ethoxy groups linked to Ti-atoms procuring a very large entropy gain.

The above conclusions were based on the assumption of the existence in solution of a $\{Ti_4O_{16}\}$ core for titanium ethoxide. There is some experimental evidence in literature supporting such an assumption as corresponding equilibrium constants have been published [69]:

$$2Ti(OEt)_4 \leftrightarrows [Ti_2(OEt)_8]K_2(C_6H_6) = 100 and K_2(dioxane) = 20$$

$$[Ti_2(OEt)_8] + Ti(OEt)_4 \leftrightarrows [Ti_3(OEt)_{12}]K_3(C_6H_6) = 110 etK_3(dioxane) = 88$$

$$[Ti_3(OEt)_{12}] + Ti(OEt)_4 \leftrightarrows [Ti_4(OEt)_{16}]K_4(C_6H_6) = K_4(dioxane) = 200$$

It was also shown through ^{1}H [68] and ^{13}C NMR [70] that the $[Ti_3(OEt)_{12}]$ trimer was unstable below –20 °C transforming most probably into the $[Ti_4(OEt)_{16}]$ tetramer known to exist in the solid state [58]. This interpretation has, however, been immediately criticized on the ground that a water concentration in benzene as low as 4×10^{-3} m was enough to explain any condensation degree above 3 [71]. In contradiction with the above values, it was shown that the condensation degree of titanium ethoxide was 2.82 in ultra-dry benzene being independent of concentration [71]. There are also some unresolved controversies about the molecular structure of such a trimer in solution. Based on XANES/EXAFS data, J. Livage's group has brought some experimental evidence for a non-centrosymmetric cyclic structure with all Ti-atoms in five-fold-coordination (named 555-isomer hereafter) in the pure liquid [59]. However, according to group theory, one would then expect in this case eight Ti—O vibrations modes of E' symmetry that are both active in IR and Raman in contradiction with IR and Raman spectra [67]. Moreover, the molecular anisotropy of $Ti(OEt)_4$ in cyclohexane or CCl_4 was also measured leading $\gamma^2 = 1.11 \times 10^{-46}$ cm^6, a value equal to that predicted ($\gamma^2 = 1.12 \times 10^{-46}$ cm^6) for a centro-symmetric structure having one Ti-atom in octahedral coordination flanked by two outer fivefold coordinated Ti-atoms (named 565-isomer hereafter) [67]. The calculated molecular anisotropy of the 555-isomer being one order of magnitude larger ($\gamma^2 = 1.4 \times 10^{-47}$ cm^6) is thus also not supported by these light scattering data, while the presence of an inversion center in the 565-isomer readily explains the lack of common bands in IR and Raman spectra. Finally, existence of the 555-isomer in benzene solutions was also not supported by recent XANES/EXAFS measurements favoring the 565-isomer [60].

With these results in mind, let the self-energy data given in Fig. 16 be applied to the equilibrium (3/4) $[Ti_4(OEt)_{16}]$ <-> $[Ti_3(OEt)_{12}]$ showing that

this entropy-driven depolymerization ($\Delta S = +94$–95 J.mol^{-1}.K^{-1}) should be an endothermic process characterized by $\Delta H = +92$ kJ.mol^{-1} for transformation of the tetramer into the 565-trimer against $\Delta H = +2350$ kJ.mol^{-1} for transformation into the 555-trimer. Considering that four ethoxy bridges are broken on going from the tetramer towards the 565-trimer, the enthalpy content of a Ti—OEt—Ti bridge may be estimated as $-\Delta H/4 = -23$ kJ.mol^{-1} in good agreement with the value -21 kJ.mol^{-1} derived from latent heat vaporization measurements [72] or the value -23 kJ.mol^{-1} derived from ^{1}H NMR data [73]. The same value derived from the 555-isomer being in complete disagreement with available experimental data, the existence of this structure in solution may be ruled out beyond any doubt on thermodynamic grounds. It is also worth noting that taking into account the entropy contribution, we still have $\Delta G_{253K} = +70$ kJ.mol^{-1} for $[Ti_4(OEt)_{16}]$ depolymerization at $T = -20$ °C. The easy destruction of the tetramer observed through ^{1}H NMR at this temperature means that another source of entropy is needed to account for this spontaneous depolymerization. As the entropy values given in Fig. 16 were derived for completely rigid structures, the additional entropy released by the free rotation of the 12 methyl groups in the 565-trimer would lead to $\Delta S = 275$ J.mol^{-1}.K^{-1}, i.e. to a predicted depolymerization temperature $T^* = 92000/275 = 335$ K not too far from the observed value $T^* = 253$ K. A slight shortening of Ti—O distances, or a difference in vibrational entropies (assumed here to be the same for the tetramer and the trimer) would easily account for the 82 K difference between theory and experiment. Consequently, in order to study the reaction of $[Ti_3(OEt)_{12}]$ with H_3bhmpc we will consider the following equation:

$$(4/3)[Ti_3(OEt)_{12}](565) + 6H_3bhmpc(inter) + 2H_2O + 2C_4H_8O_2 \rightarrow 14EtOH + \{[Ti_2O(bhmpc)(Hbhmpc)(H_2bhmpc)].C_4H_8O_2.EtOH\}_2$$

From the data given in Fig. 16, comes $\Delta H = +61$ kJ.mol^{-1} and $\Delta S = +676$ J.mol^{-1}.K^{-1} leading to $\Delta G_{300K} = -142$ kJ.mol^{-1}, showing as expected that the linear $[Ti_3(OEt)_{12}]$ trimer is more reactive than the brucitane-type $[Ti_4(OEt)_{16}]$ tetramer.

5. Conclusions

In summary, we have shown that by using a combination of X-ray diffraction, multidimensional NMR techniques and electronic density modeling, it was possible to propose a complete assignment for ^{13}C and ^{1}H solution NMR spectra of a titanium(IV) oxo-aryloxide. More specifically, it was observed that experimental X-ray diffraction data was not accurate enough to yield a direct and faithful interpretation of ^{13}C NMR data in solution. Useful correlation between a crystal structure and a solution ^{13}C NMR spectrum emerges only after some kind of averaging of metrical errors arising from the refinement process. As shown here, the PACHA formalism [34,35] may be used in conjunction with *ab initio* short-range repulsive potentials to perform this kind of averaging. Obviously, another approach would have been to use a full *ab initio* approach allowing one to perform in a single step both the necessary geometrical optimization and the evaluation of the corresponding NMR chemical shift tensors. As far as sol–gel precursors are concerned, we do prefer the PACHA approach owing to its ability to treat quickly very large systems (with several hundreds of constituent atoms) that are well beyond the scope of full *ab initio* methods. The approach used in this paper does not suffer from such limitations as it involves a combination of experimental measurements analyzed in terms of a non-empirical and quite rigorous theoretical formalism that may be easily applied even for very large unit cells. In this mixed approach, experimental data may be used to check the validity of theoretical conclusions, whereas by reciprocity the theoretical model may help to handle satisfactorily and quickly quite complex experimental situations. Another big advantage of the above approach is that it allows considering on the same theoretical grounds either isolated molecules displaying ideal geometry, either whole crystalline networks as shown here (see [74–76] for other examples related to microporous compounds). This last point is obviously of crucial importance if one is interested in assigning high-resolution solid-state ^{13}C CPMAS NMR spectra of such sol–gel precursors that very often display a very large number of well-resolved signals. Yet another nice feature of the presented approach is the possibility to perform a full thermodynamic analysis of the chemical modification of alkoxides precursors putting on a quantitative basis the link between molecular structure in solution and chemical reactivity. This triple treatment of sol–gel precursors based on powerful spectroscopic measurements, electronic density modeling and rigorous statistical thermodynamic considerations was initiated about 25 five years ago under the

scientific supervision of J. Livage and the Strasbourg's group is very happy to honor him by this contribution for his 70th birthday.

References

[1] M. Henry, in : H.S. Nalwa (Ed.), Handbook of Organic–Inorganic Hybrid Materials and Nanocomposites, 1, American Scientific Publisher, Stevenson Ranch, 2003, p. 1.
[2] R. Janes, M. Edge, J. Rigby, D. Mourelatou, N.S. Allen, Dyes Pigments 48 (2001) 29.
[3] H. Schroeder, Physics of Thin Films, 5, Academic Press, New-York, 1969, 87.
[4] J. Pascual, J. Camassel, H. Mathieu, Phys. Rev. B 18 (1978) 5606.
[5] A. Fujishima, K. Honda, Nature 238 (1972) 37.
[6] J. Ovenstone, K. Yanagisawa, Chem. Mater. 11 (1999) 2770.
[7] H. Tang, K. Prasad, S. Sanjinés, F. Lévy, Sens. Actuators B 26 (1995) 71.
[8] M. Grätzel, Nature 414 (2001) 338.
[9] R. Wang, K. Hashimoto, A. Fujishima, Adv. Mater. 2 (1998) 135.
[10] D. Hennings, M. Klee, R. Waser, Chem. Mater 3 (1991) 334.
[11] C.D. Chandler, M.J. Hampden-Smith, Chem. Mater 4 (1992) 1137.
[12] C.D. Chandler, C. Roger, M.J. Hampden-Smith, Chem. Rev 93 (1993) 1205.
[13] G. Schottner, Chem. Mater 13 (2001) 3422.
[14] M. Henry, A. Vioux, J. Livage, ANVAR Patent n° 85-12019, 6-08-1985.
[15] S. Doeuff, M. Henry, C. Sanchez, J. Livage, J. Non-Cryst. Solids 89 (1987) 84.
[16] S. Doeuff, M. Henry, C. Sanchez, J. Livage, J. Non-Cryst. Solids 89 (1987) 206.
[17] J. Livage, C. Sanchez, M. Henry, S. Doeuff, Solid State Ionics 32–33 (1989) 633.
[18] S. Doeuff, M. Henry, C. Sanchez, Mat. Res. Bull. 25 (1990) 1519.
[19] S. Doeuff, M. Henry, C. Sanchez, Mat. Res. Soc. Symp. Proc. 73 (1986) 653.
[20] J. Livage, M. Henry, in : J.D. Mackenzie, D.R. Ulrich (Eds.), Ultrastructure Processing of Advanced Ceramics, Wiley, New-York, 1988, p. 183.
[21] C. Sanchez, J. Livage, M. Henry, F. Babonneau, J. Non-Cryst. Solids 100 (1988) 65.
[22] J. Livage, M. Henry, C. Sanchez, Prog. Solid State Chem. 18 (1988) 259.
[23] J. Livage, M. Henry, J.P. Jolivet, in : L.L. Hench, J.K. West (Eds.), Chemical Processing of Advanced Materials, Wiley, New-York, 1992, p. 223.
[24] L. Moens, P. Ruiz, R. Delmon, M. Devillers, Appl. Catal. A: Gen. 249 (2003) 365.
[25] J.G. Reynolds, Silicon Chem. 3 (2005) 267.
[26] L. Weng, K. Sagoe-Crentsil, T. Brown, S. Song, Mat. Sci. Eng. B 117 (2005) 163.
[27] L. Weng, S.N.B. Hodgson, J. Non-Cryst. Solids 297 (2002) 18.
[28] T.J. Boyle, T.M. Alam, E.R. Mechenbier, B.L. Scott, J.W. Ziller, Inorg. Chem. 36 (1997) 3293.
[29] H.A. Christ, P. Diehl, H.R. Schneider, H. Dahn, Helv. Chim. Acta 44 (1961) 865.
[30] J. Blanchard, S. Barboux-Doeuff, J. Maquet, C. Sanchez, New J. Chem. 19 (1995) 929–941.
[31] V.W. Day, T.A. Eberspacher, W.G. Klemperer, C.W. Park, F.S. Rosenberg, J. Am. Chem. Soc. 113 (1991) 8190.
[32] G.J.A.A. Soler-Illia, E. Scolan, A. Louis, P.A. Albouy, C. Sanchez, New J. Chem. 25 (2001) 156.
[33] A. Rammal, F. Brisach, M. Henry, J. Am. Chem. Soc. 123 (2001) 5612.
[34] M. Henry, CHEMPHYSCHEM 3 (2002) 561.
[35] M. Henry, in : V. Mihai, Putz (Eds.), Advances in Quantum Chemical Bonding Structures, Transworld Research Network, Kerala, India, 2008, p. 153.
[36] D.R. Lide (Ed.), Handbook of Chemistry and Physics, 81st edition (2000-2001), CRC Press, Boca Raton, 2000, , 9-1.
[37] M.A. Spackman, J. Chem. Phys. 85 (1986) 6579.
[38] F. Biechel, J. Dubuc, M. Henry, New J. Chem. 28 (2004) 764.
[39] M. Henry, CHEMPHYSCHEM 3 (2002) 607.
[40] M. Henry, C. Gérardin, F. Taulelle, Mater. Res. Soc. Symp. Proc. 271 (1992) 243.
[41] C. Gérardin, M. Henry, F. Taulelle, Mater. Res. Soc. Symp. Proc. 271 (1992) 777.
[42] C. Gérardin, M. Henry, F. Taulelle, in : J.A. Tossell (Ed.), Nuclear Magnetic Shieldings and Molecular Structure, NATO-ASI Series C, 386, Kluwer, Dordrecht, 1993, p. 566.
[43] M. Henry, Mater. Sci. Forum 152–153 (1994) 355.
[44] M. Henry, ACS Symp. Ser. 732 (1999) 277.
[45] T.M. Alam, M. Henry, Phys. Chem. Chem. Phys. 2 (2000) 23.
[46] A. Senouci, M. Yaakoub, C. Huguenard, M. Henry, J. Mater. Chem. 14 (2004) 3215.
[47] A.K. Jameson, C.J. Jameson, Chem. Phys. Lett. 134 (1987) 461.
[48] K.M.S. Saxena, P.T. Narasimhan, Int. J. Quantum Chem. 1 (1967) 731.
[49] R.G. Barnes, W.V. Smith, Phys. Rev. 93 (1954) 95.
[50] J.A. Pople, Mol. Phys. 7 (1963) 301.
[51] M. Karplus, J.A. Pople, J. Chem. Phys. 38 (1963) 2803.
[52] F. Hynne, K. Andersen, Am. J. Phys. 47 (1979) 649.
[53] M.C. Gupta, Statistical Thermodynamics, 2nd Ed., New Age International, New Dehli, 1990, 232.
[54] R.E. Powell, W.M. Latimer, J. Chem. Phys. 19 (1954) 1139.
[55] A.G. Csaszar, G. Czako, T. Furtenbacher, J. Tennyson, V. Szalay, S.V. Shirin, N.F. Zobov, O.L. Polyanski, J. Chem. Phys. 112 (2005) 214305.
[56] http://riodb01.ibase.aist.go.jp/sdbs/cgi-bin/cre_index.cgi.
[57] D.A. Wright, D.A. Williams, Acta Cryst. B 24 (1968) 1107.
[58] J.A. Ibers, Nature 197 (1963) 686.
[59] F. Babonneau, S. Doeuff, A. Leaustic, C. Sanchez, C. Cartier, M. Verdaguer, Inorg. Chem. 27 (1988) 3166.
[60] M. Bauer, G. Kickelbick, E. Wendel, V. Krishnan, H. Bertagnolli, Report for HASYLAB Jahresbericht (2004). http://hasyweb.desy.de/science/annual_reports/2004_report/part1/contrib/41/11954.pdf.
[61] http://www.sigmaaldrich.com.
[62] Yu.N. Levchuk, N.V. Kuznetsov, I.I. Krasavtev, J. Appl. Spectroc. 17 (1972) 1055.
[63] S.P.S. Porto, P.A. Fleury, T.C. Damen, Phys. Rev. 154 (1967) 522.
[64] D.A. Ramsay, Proc. R. Soc. London A 190 (1947) 562.
[65] J. Guimont, O. Poncelet, J. Rigola, S. Truchet, Vib. Spectrosc. 11 (1996) 37.
[66] G. Malli, S. Fraga, Theoret. Chim. Acta 6 (1966) 54.
[67] W.R. Russo, W.H. Nelson, J. Am. Chem. Soc. 92 (1970) 1521.
[68] D.C. Bradley, C.E. Holloway, J. Chem. Soc. (A) (1968) 1316.
[69] C.G. Barraclough, R.L. Martin, G. Winter, J. Chem. Soc. (1964) 758.

[70] C. E. Holloway, J. Chem. Soc. Dalton Trans. Dalton, (1976) 1050.
[71] D.C. Bradley, C.E. Holloway, Inorg. Chem. 3 (1964) 1163.
[72] D.C. Bradley, R.C. Mehrotra, W. Wardlaw, J. Chem. Soc. (1953) 2025.
[73] H. Weingarten, J.R. Van Wazer, J. Am. Chem. Soc. 87 (1965) 724.
[74] L. Beitone, J. Marrot, T. Loiseau, G. Férey, M. Henry, C. Huguenard, A. Gansmuller, F. Taulelle, J. Am. Chem. Soc. 125 (2003) 1912.
[75] L. Beitone, C. Huguenard, A. Gansmüller, M. Henry, F. Taulelle, T. Loiseau, G. Férey, J. Am. Chem. Soc. 125 (2003) 9102.
[76] T. Loiseau, C. Serre, C. Huguenard, G. Fink, F. Taulelle, M. Henry, T. Bataille, G. Férey, Chem. Eur. J. 10 (2004) 1373.